PHYSICAL REVIEW D **95,** 076016 (2017)

Efficient evaluation of massive Mellin-Barnes integrals

Janusz Gluza and Tomasz Jeliński
Department of Field Theory and Particle Physics, Institute of Physics, University of Silesia, Uniwersytecka 4, PL–40-007 Katowice, Poland

David A. Kosower
School of Natural Sciences, Institute for Advanced Study, 1 Einstein Drive, Princeton, New Jersey 08540, USA and Institut de Physique Théorique, CEA, CNRS, Université Paris–Saclay, F–91191 Gif-sur-Yvette cedex, France

(Received 28 November 2016; published 24 April 2017)

We show how to evaluate one-dimensional Minkowski-region Mellin-Barnes representations arising from massive loop integrals, by modifying the contours of integration. We implement an exact solution to the differential equation determining the contours of stationary phase. We also present several simple approximations to these contours. Our approach points the way to more efficient computations of massless and massive Mellin-Barnes integrals in both Euclidean and Minkowski regions.

DOI: 10.1103/PhysRevD.95.076016

I. INTRODUCTION

The Mellin-Barnes approach has proven to be a versatile and successful approach to evaluating higher-loop integrals, both analytically and numerically [1,2]. Its early successes included the analytic computation of the planar [3] and nonplanar [4] two-loop double-box integrals. In this approach, one first introduces a Feynman parametrization into loop integrals, performs the loop integrals, and then uses Mellin-Barnes representations for the integrands to allow the Feynman parameter integrals to be computed. The integrals are typically infrared divergent and may have ultraviolet divergences as well. These divergences are usually regulated dimensionally; the resulting singularities are hidden inside the integrands of the Mellin-Barnes integrals. One can move the contours to make these singularities manifest, yielding a representation in which the poles in the regulator ϵ are manifest and in which the coefficients are finite Mellin-Barnes integrals which can be computed analytically or numerically. Czakon's MB package [5] automated the process of moving contours to resolve singularities; a related algorithm was later implemented in MBresolve by Smirnov and Smirnov [6]. Other publicly available packages connected with the Mellin-Barnes evaluation of Feynman integrals are available on the MBtools web page [7]: AMBRE [8,9], which assists in creating Mellin-Barnes representations; MBasymptotics [10], which performs parametric expansions of Mellin-Barnes integrals; and barnesroutines [11], which automates the application of Barnes lemmas. The use of Mellin-Barnes representations goes back much further than these developments; in Refs. [12–14], Mellin-Barnes representations were used for massive propagators.

The Mellin-Barnes approach has been used extensively for numerical cross-checks of analytic results in the Euclidean region, including in two-loop massive Bhabha scattering in QED [15]; in three-loop massless form factors [16] and static potentials [17]; in massive two-loop QCD form factors [18]; in B-physics studies [19]; in hadronic top-quark physics [20]; and for angular integrations in phase-space integrals [21]. It has also been used to obtain direct numerical results in computations in supersymmetric Yang-Mills theories: for the four-loop cusp anomalous dimension [22] and two-loop five-point amplitudes [23]; as well as in $\mathcal{N} = 6$ Chern-Simons theory at six loops and beyond [24]. Very recently, it has been applied to integrals in chiral perturbation theory [25].

The MB and MBresolve packages yield numerically convergent integrals in the Euclidean region for integrals arising from a mixture of massless and massive propagators. The same integrals are typically only conditionally convergent in the Minkowski region and, hence, fail to converge numerically. For Feynman integrals that arise at one loop, one can ultimately perform the integrations analytically and assemble these results into numerical software libraries [26–30]. The convergence failure is then an annoyance and prevents use of numerical approaches as cross-checks, but it is not a critical problem.

At two loops and beyond, not all desired integrals are available analytically, and the obstruction is of greater importance. A variety of other techniques can be applied to the numerical calculation of Feynman integrals in the Minkowski region. These include sector decomposition [31] (as implemented, for example, in SecDec 3 [32–34] and Fiesta 4 [35]); numerical subtraction of singularities in loop-momentum space [36–41], along with appropriate complex contour deformations of the Feynman-parameter integrations. (See Refs. [37,42–45] for earlier one-loop results.)

The Mellin-Barnes integrals produced by the MB and MBresolve packages use standard contours, parallel to the

imaginary axis. The representation was re-examined by Freitas and Huang [46], who pointed out that using tilted contours of integration different from the textbook contours chosen by MB can make Minkowski-region massive integrals convergent. These authors did not specify exactly how these tilted linear contours should be chosen. A recent Mellin-Barnes-based numerical package, MBnumerics [47], takes a different approach, shifting and rotating contours, remapping integrands, and dropping small contributions to compute multidimensional integrals with multiple scales in the Minkowski region [9]. It has been applied to the two-loop bosonic contributions to $Z \to b\bar{b}$ [48].

In this article, we re-examine the choice of contours, and show how to determine contours that are in a certain sense close approximations to optimal contours of integration. We study one-dimensional Mellin-Barnes integrals both in the Euclidean and Minkowski regions. Our contours improve the numerical efficiency of computation in the former region, and provide an efficient and convergent representation in the latter. We also present a connection to the tilted contours suggested by Freitas and Huang [46]. While these contours are not computationally optimal, they do have the virtue of simplicity. We believe that the approach described here will generalize to higher-dimensional Mellin-Barnes integrals; but the generalization is not trivial nor completely straightforward, and accordingly we postpone any discussion of it to future work.

This article is organized as follows. In the next section, we study an example of a one-dimensional massive integral in the Euclidean region. We also discuss the differential equation drawn from the mathematics literature which determines an exact contour of stationary phase. In Sec. III, we present several approximations to the exact contour, for parameter values in the Euclidean region. In Sec. IV, we show how to match contours to their asymptotic forms, and in Sec. V, we give examples of various use cases exemplifying the utility of using approximate contours and matching to their asymptotic forms. We use as examples integrals that may arise in Feynman diagrams. In Sec. VI, we study approximations to contours of stationary phase for parameters in the Minkowski region. In Sec. VII, we examine one important special case, of integrals with no stationary point along the real axis even for parameters in the Euclidean region. In Sec. VIII, we examine briefly the evaluation of integrals using the various contour approximations discussed in earlier sections. We give some concluding remarks in Sec. IX.

II. A EUCLIDEAN INTEGRAL

Let us begin by studying Mellin-Barnes integrals in the Euclidean region. In this region, the standard contours used in the definition of the integrals—as well as by the MB package—are usually suitable for numerical integration as well. But we can improve upon them, and the improvements offer a stepping stone to the modifications required to obtain a numerically convergent form in the Minkowski region.

We begin with a one-dimensional integral,

$$I_1(s) = \frac{1}{2\pi i}\int_{c_0-i\infty}^{c_0+i\infty} dz F_1(z,s), \tag{2.1}$$

where

$$F_1(z,s) = (-s)^{-z}\frac{\Gamma^3(-z)\Gamma(1+z)}{\Gamma(-2z)}. \tag{2.2}$$

This integral was considered in Refs. [5,9]. As mentioned there, it can be evaluated analytically, with result,

$$\frac{4}{\sqrt{\frac{4}{-s}+1}}\operatorname{asinh}\sqrt{-\frac{s}{4}}, \tag{2.3}$$

in the Euclidean region $s < 0$;

$$-\frac{4}{\sqrt{\frac{4}{s}-1}}\operatorname{asin}\sqrt{\frac{s}{4}}, \tag{2.4}$$

below threshold ($s \in [0,4]$) in the Minkowski region; and,

$$\frac{4}{\sqrt{1-\frac{4}{s}}}\left[-\frac{i\pi}{2}\operatorname{sign}\operatorname{Im} s + \ln\left(\sqrt{\frac{s}{4}}+\sqrt{\frac{s}{4}-1}\right)\right], \tag{2.5}$$

above threshold. (The forms in Eqs. (2.4) and (2.5) correspond to Eq. (2.3) when s is given a small imaginary part.)

In the Euclidean region, $s < 0$, and hence the integrand is real for real z. The reflection symmetry $z \leftrightarrow \bar{z}$ then ensures the integral is real as well. The MB package, left to its own devices, will choose $c_0 = -\frac{1}{2}$. Let us consider the integral for $s = -\frac{1}{20}$. The real and imaginary parts of the integrand along the contour are shown in Fig. 1. Both oscillate around zero, though the oscillations are damped as one moves away from the real axis, and the resulting numerical integral converges nicely. (Obtaining the vanishing result for the imaginary part does require nontrivial cancellations in a numerical integration, of course.)

Nonetheless, let us ask: why choose this particular contour? Or, more pointedly: can we do any better? Is there a more efficient contour?

Complex-analysis textbooks would tell us that the answer is yes: we should choose the contour of steepest descent. This will yield the most-rapidly convergent integral, because it is also a contour of stationary phase and hence minimizes oscillations in the integrand. Figure 2 shows a variety of contours of stationary phase for the integrand $F_1(z, s = -\frac{1}{20})$; in the case at hand, we should pick the contour of phase 0. As in the case of parton-distribution evolution [49], we must face the questions of

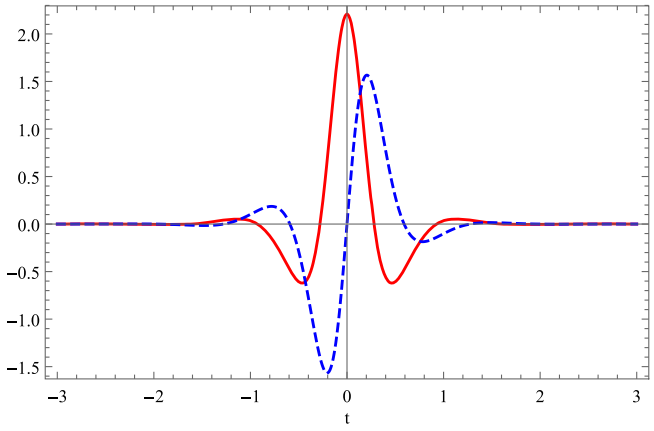

FIG. 1. The real (red) and imaginary (dashed blue) parts of the integrand $F_1(z,s)$ of Eq. (2.2) for $s=-\frac{1}{20}$ along the "textbook" (and MB) contour, $\mathrm{Re}\, z = c_0 = -\frac{1}{2}$.

whether we can find a good approximation to this contour without undue computational effort; and whether we can easily adapt the contour to different values of the parameter s. As we shall see, we can provide affirmative answers to both questions.

Our first task in finding the contour of stationary phase in this case is to find a local minimum along the real axis. The minimum closest to $z=-\frac{1}{2}$ is given by the solution to,

$$-\ln(-s)+2\psi(-2z)-3\psi(-z)+\psi(z+1)=0, \quad (2.6)$$

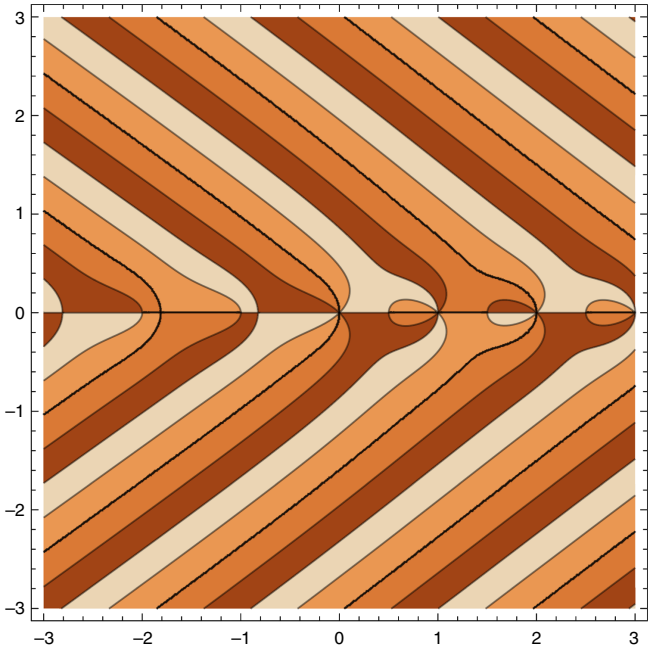

FIG. 2. A contour plot of phases for the integrand $F_1(z,s)$ of Eq. (2.2) with $s=-\frac{1}{20}$, with contours for phases $-\pi/2$, 0, $\pi/2$, and π also shown. The contour with phase 0 is the boundary between the darkest and lightest shade.

which is at $z_s \simeq -0.825618$ for $s=-\frac{1}{20}$. Because we have the analytic form of the integrand, we can easily obtain this equation analytically, and then use an efficient algorithm (e.g. Newton-Raphson) to find a numerical solution.

Before looking at a sequence of approximations to the desired contour, let us examine the exact contour $z(t)$, anchored at the above minimum. In the present case, $\mathrm{Im}\, F_1(z,s)$ will vanish exactly along the contour. We seek contours described by a meromorphic function; and F_1 itself is meromorphic as well. The contour then satisfies a differential equation [50],

$$\frac{dz}{dt} = -\overline{\frac{\partial \ln F_1(z,s)}{\partial z}}. \quad (2.7)$$

The phase of F_1 is given by $\mathrm{Im}\ln F_1$; along a contour satisfying Eq. (2.7), the phase does not vary,

$$\begin{aligned}\frac{d\,\mathrm{phase}}{dt} &= \frac{d\,\mathrm{Im}\ln F_1}{dt} = \frac{1}{2i}\left[\frac{d\ln F_1}{dt}-\frac{d\ln \overline{F_1}}{dt}\right]\\ &= \frac{1}{2i}\left[\frac{\partial \ln F_1}{\partial z}\frac{dz}{dt}-\overline{\frac{\partial \ln F_1}{\partial z}}\frac{d\bar{z}}{dt}\right]\\ &= -\frac{1}{2i}\left[\frac{\partial \ln F_1}{\partial z}\overline{\frac{\partial \ln F_1}{\partial z}}-\overline{\frac{\partial \ln F_1}{\partial z}}\frac{\partial \ln F_1}{\partial z}\right]\\ &= 0. \end{aligned} \quad (2.8)$$

Furthermore,

$$\begin{aligned}\frac{d|F_1|^2}{dt} &= |F_1|^2\left[\frac{d\ln F_1}{dt}+\frac{d\ln \overline{F_1}}{dt}\right]\\ &= |F_1|^2\left[\frac{\partial \ln F_1}{\partial z}\frac{dz}{dt}+\overline{\frac{\partial \ln F_1}{\partial z}}\frac{d\bar{z}}{dt}\right]\\ &= -|F_1|^2\left[\frac{\partial \ln F_1}{\partial z}\overline{\frac{\partial \ln F_1}{\partial z}}+\overline{\frac{\partial \ln F_1}{\partial z}}\frac{\partial \ln F_1}{\partial z}\right]\\ &= -2|F_1|^2\left|\frac{\partial \ln F_1}{\partial z}\right|^2 < 0, \end{aligned} \quad (2.9)$$

so that as expected it is a contour of steepest descent.

The stationary point z_s is also a stationary point of this equation; a solution which starts at z_s will stay there for all t. As boundary data for the differential equation, we must therefore choose a different point. A suitable choice is given by perturbing away from z_s along one of the two directions of steepest descent. In general, one can find these by finding the eigenvectors of the Hessian of the integrand; in this case, the required directions are parallel to the imaginary axis, in either the positive and negative direction. One can then solve the equation numerically; one must do so separately in the upper- and lower-half planes. (Alternatively, in the Euclidean region the lower half-plane contour will be the complex conjugate of the upper half-plane contour.) The pair of contours together

is called the Lefschetz thimble $\mathcal{J}(z_s)$ associated to the stationary point z_s.

In the case at hand, one starts with z_s as given by the solution to Eq. (2.6) and looks for the tangent to it. For Euclidean values of s, the line $\mathrm{Re}\, z = z_s$ will be that tangent, because a minimum along the real axis is a saddle point of the integrand in the complex plane. We can perturb away from the stationary point along the tangent,

$$z_s(\delta) = z_s + i\delta, \tag{2.10}$$

in order to obtain a suitable starting point for the differential equation. (The smaller δ, the more accurate the solution will be.) We make use of the MATHEMATICA routine NDSolve to solve the differential equation Eq. (2.7) with starting points $z_s(\pm\delta)$. This yields a numerical representation of the exact contour of stationary phase. We show examples of exact contours in the following sections.

In general, however, solving the differential equation (2.7), and then using the solution repeatedly in a numerical integration, may be computationally expensive. Furthermore, we may encounter integrals for which the exact contour of stationary phase is not optimal for numerical integration, and where the MB integral would require special treatment with an exact contour. This motivates us to seek approximations to the exact contour of stationary phase, which we consider in the next section.

III. CONTOUR APPROXIMATIONS

The simplest approximation to the exact contour of stationary phase is given by a straight line tangent to it. As noted in the previous section, the line $\mathrm{Re}\, z = z_s$ will be that tangent. If we take our contour to be this line, we see that while the integrand still oscillates (see Fig. 3), the oscillations are damped more quickly than along the original contour.

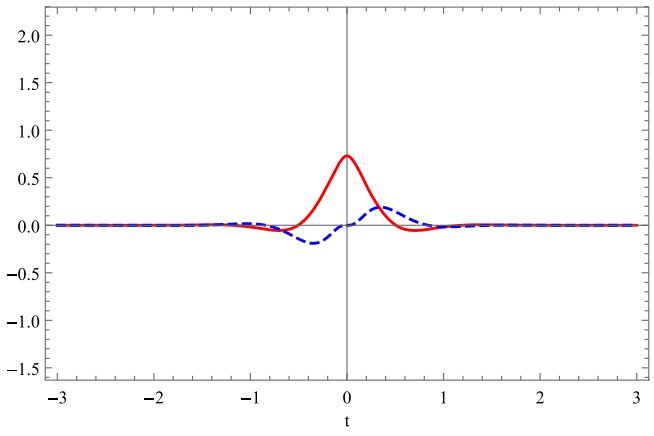

FIG. 3. The real (red) and imaginary (dashed blue) parts of the integrand $F_1(z,s)$ of Eq. (2.2) for $s = -\frac{1}{20}$ along the contour $\mathrm{Re}\, z = -0.825618$, tangent to the contour of steepest descent.

We can improve on the tangent approximation; to find a better approximation, we follow the same procedure as in Ref. [49]. Parametrize $z(t) = x(t) + iy(t)$, choosing

$$x(t_0 = 0) = z_s, \qquad y(0) = 0, \qquad x, y \text{ real}. \tag{3.1}$$

If we require the contour to be symmetric under reflection in the real axis (as is desirable for numerical evaluation), x will be an even function, and y an odd one. We can rescale t to make $y'(0) = 1$. Taking the contour to be smooth, we will also have $x'(0) = 0$. The expansion of the integrand around $z = z_s$ then takes the form,

$$\begin{aligned} F_1(z(t)) &\sim F_1(z_s) + \frac{F_1''(z_s)}{2} \\ &\quad \times (x'(0)^2 - y'(0)^2 + 2ix'(0)y'(0))t^2 + \cdots \\ &= F_1(z_s) - \frac{F_1''(z_s)}{2} t^2 + \cdots \end{aligned} \tag{3.2}$$

where we drop the s argument for brevity. As all derivatives of $F_1(x)$ are real, the equation $\mathrm{Im}\, F_1(z(t)) = 0$ is satisfied to this order; and as $F_1''(z_s)$ is positive, the integrand decreases with t. However, the contour will not continue parallel to the imaginary axis; to see where it goes, we must expand to higher order. Consider the expansion to $\mathcal{O}(t^3)$,

$$\begin{aligned} F_1(z(t)) &\sim F_1(z_s) - \frac{F_1''(z_s)}{2} t^2 \\ &\quad + \frac{1}{6}\left(-iF_1^{(3)}(z_s) + 3iF_1''(z_s)x''(0)\right)t^3 + \cdots \end{aligned} \tag{3.3}$$

To this order, the stationary-phase condition ($\mathrm{Im}\, F_1(z(t)) = 0$) requires,

$$x''(0) = \frac{F_1^{(3)}(z_s)}{3F_1''(z_s)}. \tag{3.4}$$

In the neighborhood of z_s, the approximate contour then has the form,

$$z_q(t) = z_s + it + c_2 t^2, \tag{3.5}$$

where c_2 is real, and given by,

$$c_2 = \frac{F_1^{(3)}(z_s)}{6F_1''(z_s)}. \tag{3.6}$$

Because $x^{(3)}(0)$ vanishes, the terms of $\mathcal{O}(t^4)$ are automatically real, and only at $\mathcal{O}(t^5)$ do imaginary terms now appear in the expansion of $F(z(t))$.

In the example at hand ($s = -\frac{1}{20}$), the quadratic contour is,

$$z_q(t) = -0.825618 + it - 1.65358t^2. \tag{3.7}$$

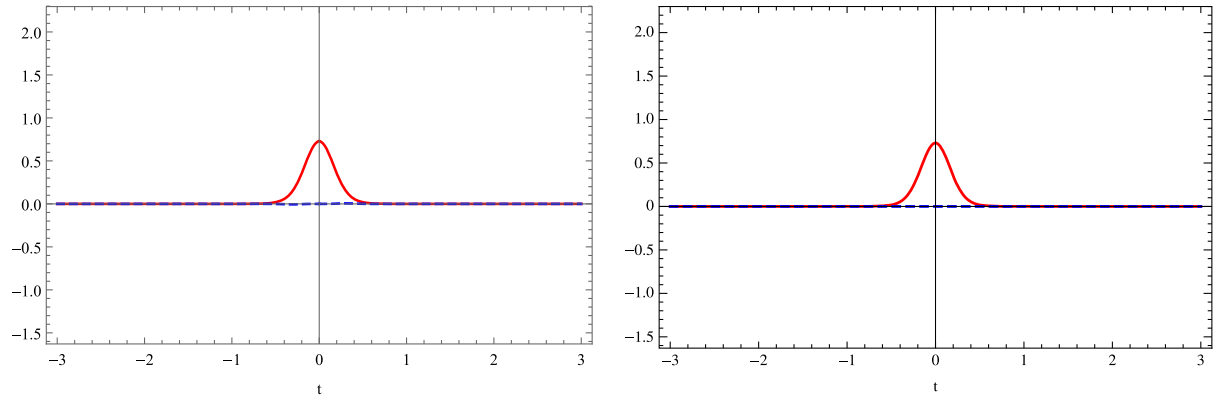

FIG. 4. The real (red) and imaginary (dashed blue) parts of the integrand $F_1(z,s)$ of Eq. (2.2) for $s=-\frac{1}{20}$ along (a) the quadratic approximation $z_q(t)$ to the contour of stationary phase (b) the exact contour.

The value of the integrand along the contour is shown in Fig. 4(a). The imaginary part is essentially zero, and the real part is free of oscillations in the region which gives the bulk of the contributions to the result. (The parametrized integrand will still have an imaginary part, because of the $z'(t)$ factor, but there is no need to compute it.) For comparison, in Fig. 4(b), we show the integrand along the exact contour of stationary phase, computed using the differential equation as described in Sec. II. The imaginary part of the contour is chosen to be t in both figures.

The two linear contours (original and tangent) and the quadratic contour are shown along with the exact contours of stationary phase in Fig. 5.

There is another improvement we can make to the contour. Notice that the contours of constant phase, shown in Fig. 2, are all asymptotically straight lines as $z\to\infty$ (so long as we stay away from the real axis). We can see this analytically by using the asymptotic expansion of the gamma function,

$$\Gamma(z)\overset{z\to\infty}{\sim}\sqrt{\frac{2\pi}{z}}z^z e^{-z}, \tag{3.8}$$

in Eq. (2.2) to obtain an asymptotic form for the integrand (with $s<0$),

$$F\sim \text{const}\, 4^z(-s)^{-z}\frac{(1+z)^{1/2+z}}{(-z)^{1+z}}; \tag{3.9}$$

paying careful attention to the branch cuts, we can further simplify this expression to obtain,

$$F\sim \text{const}\, 4^z(-s)^{-z}\frac{(-1+i\delta\,\text{sign}\,\text{Im}\,z)^{z+1/2}}{\sqrt{-z}}, \tag{3.10}$$

where δ is an infinitesimal positive number.

We can compute the phase of this expression via,

$$\arg(z)=-i\ln(z/|z|), \tag{3.11}$$

to obtain,

$$\arg F=\frac{\pi}{2}-\frac{1}{2}\arg(-z)+\pi\,\text{Re}\;z\;\text{sign}\,\text{Im}\,z+\text{Im}\,z\ln\left(-\frac{4}{s}\right) \tag{3.12}$$

(implicitly taken mod 2π), which indeed is a linear equation as $z\to\infty$.

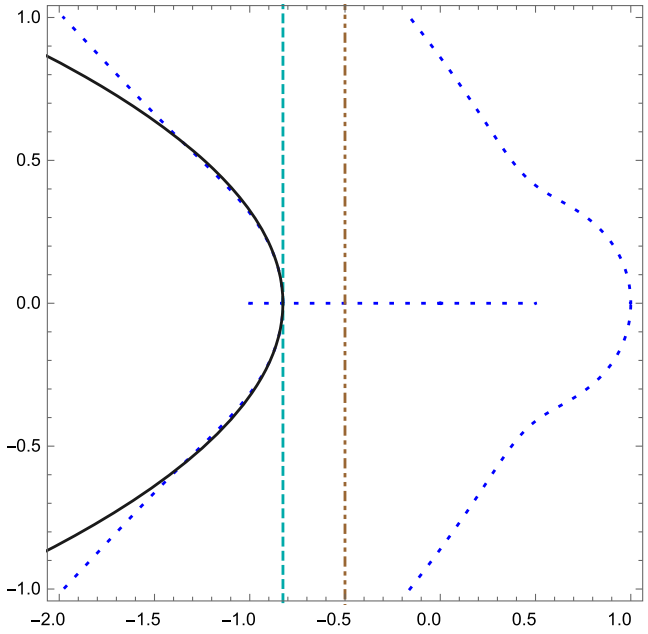

FIG. 5. The original linear (double-dot dashed brown), tangent (dashed dark turquoise), and quadratic (dot-dashed dark gray) contours for the integrand $F_1(z,s)$ of Eq. (2.2) with $s=-\frac{1}{20}$, shown along with the exact contours of zero phase (dotted blue).

Let us write the asymptotic form of the contour in the following form,

$$z_\infty(t) = \begin{cases} z_\infty + ire^{i\theta_\infty} t, & t > 0, \\ z_\infty + ire^{-i\theta_\infty} t, & t < 0, \end{cases} \tag{3.13}$$

where r is real. In this parametrization, $\theta_\infty \in [-\frac{\pi}{2}, \frac{\pi}{2}]$, with $\theta_\infty = 0$ corresponding to a line parallel to the imaginary axis. To fix the parameters z_∞ and θ_∞, substitute this form into Eq. (3.12), and expand as $t \to \infty$. Requiring the coefficient of t to vanish yields an equation for θ_∞,

$$\theta_\infty = \operatorname{atan}\left[\frac{1}{\pi}\ln(-4/s)\right]. \tag{3.14}$$

Taking the limit $t \to \infty$ in $\arg(-z)$, but setting $t = 0$ elsewhere then allows us to solve for z_∞,

$$z_\infty = -\frac{3}{4} + \frac{\theta_\infty}{2\pi}. \tag{3.15}$$

Of course, there are many contours of zero phase, as seen in Fig. 2; all asymptotic lines will share the same θ_∞, but each will have a different z_∞. The different z_∞ values will be separated by even integers; the one chosen here is the one lying in the original interval of interest $(-1, 0)$.

We will give a more general discussion of the asymptotic forms in the next section, where we consider a more general ratio of gamma functions, and additional factors of polygamma functions. Such additional factors will not affect the leading terms in the phase, and hence will leave the angle θ_∞ unchanged; they will however affect the position of the intercept z_∞.

To combine the quadratic contour with the asymptotic contour, we can replace the quadratic form in Eq. (3.5) with a Padé approximation. We need a sufficient number of coefficients to fix two angles (the tangents at the stationary point and at infinity), two intercepts (with corresponding complex parts set to zero), and the quadratic behavior of the curve (again with vanishing imaginary part). This corresponds to eight real degrees of freedom. While a $[2/1]$ Padé does allow for four complex or eight real coefficients, we can remove one real parameter by rescaling the curve parameter t, which leaves us with too few coefficients to fix in order to match the behaviors at both small and large t. Instead we use a $[3/2]$ Padé approximation. For convenience, we write it in the following form,

$$z_p(t) = \begin{cases} z_s + it + \dfrac{t^2(a_2 + ib_2 a_3 t)}{1 + ib_1 t + b_2 t^2}, & t > 0, \\ z_s + it + \dfrac{t^2(a_2^* + ib_2^* a_3^* t)}{1 + ib_1^* t + b_2^* t^2}, & t < 0, \end{cases} \tag{3.16}$$

which ensures the correct symmetry under reflection through the real axis. Matching coefficients as $t \to 0$, we find that

$$a_2 = c_2. \tag{3.17}$$

Defining

$$\begin{aligned} \tau_E &= 1 - e^{i\theta_\infty}\rho, \\ d_E &= \tau_E^2 + c_2(z_s - z_\infty), \end{aligned} \tag{3.18}$$

and also matching the leading coefficient as $t \to \infty$, we find that

$$a_3 = -\tau_E. \tag{3.19}$$

The ρ parameter corresponds to the magnitude of the coefficient in the leading $t \to \infty$ coefficient; in general, it does not appear possible to use it to improve the contour for practical purposes beyond the constraints described below, and so we simply set it to 1 here and in all following equations for the parameters in Eq. (3.16). Matching the next-to-leading coefficient as $t \to \infty$, we obtain,

$$b_1 = \frac{c_2 + b_2(z_s - z_\infty)}{\tau_E}, \tag{3.20}$$

where b_2 will be given below. Matching only through $\mathcal{O}(t^2)$ at small t would leave one complex parameter completely unfixed. We can choose it so that the integrand is real through $\mathcal{O}(t^5)$. The quartic order gives a linear equation which can be solved for the real part of b_2 in terms of its imaginary part,

$$\begin{aligned} \operatorname{Re} b_2 = {} & \frac{1}{\operatorname{Re} d_E - 2(\operatorname{Re}\tau_E)^2} \\ & \times [-c_2^2 + \operatorname{Im} b_2 \operatorname{Re}\tau_E (\operatorname{Re} d_E + 2(\operatorname{Im}\tau_E)^2)/\operatorname{Im}\tau_E], \end{aligned} \tag{3.21}$$

while the quintic order then gives a quadratic equation for the imaginary part,

$$q_2(\operatorname{Im} b_2)^2 + q_1 \operatorname{Im} b_2 + q_0 = 0. \tag{3.22}$$

Define

$$\begin{aligned} c_j &= \frac{F_1^{(j+1)}(z_s)}{(j+1)! F_1''(z_s)}, \\ f_E &= (\operatorname{Re} d_E)^2 + 4(\operatorname{Im}\tau_E \operatorname{Re}\tau_E)^2; \end{aligned} \tag{3.23}$$

the coefficients in Eq. (3.20) are then

$$\begin{aligned} q_0 = {} & c_2^4 (\operatorname{Im}\tau_E)^2 \operatorname{Re} d_E (1 - \operatorname{Re}\tau_E) \\ & + c_2 (3c_2^3 - 4c_2 c_3 + c_4)(\operatorname{Im}\tau_E)^2 \operatorname{Re} d_E (\operatorname{Re} d_E - 4(\operatorname{Re}\tau_E)^2) \\ & - 4c_2 (\operatorname{Im}\tau_E \operatorname{Re}\tau_E)^2 (c_2^3 - 2c_2^3 \operatorname{Re}\tau_E \\ & - (3c_2^3 - 4c_2 c_3 + c_4)(\operatorname{Re}\tau_E)^2), \\ q_1 = {} & 2c_2^2 \operatorname{Im}\tau_E f_E [(\operatorname{Re}\tau_E - 2(\operatorname{Re}\tau_E)^2 + \operatorname{Re} d_E], \\ q_2 = {} & -\operatorname{Re} d_E f_E [(\operatorname{Im}\tau_E)^2 - (\operatorname{Re}\tau_E)^2 + \operatorname{Re} d_E]. \end{aligned} \tag{3.24}$$

A reasonable heuristic is to take the smaller of two positive solutions; to take the positive solution if one is negative; and to take the solution of smaller magnitude if both are negative. (If the solutions are complex, take the common real part.)

In the example at hand, this curve is

$$-0.825618 + it + \frac{(-1.65358-(7.03903 + 6.94838i\,\mathrm{sign}t)|t|)t^2}{1 + (4.25685-1.28081i\,\mathrm{sign}t)|t| + (10.32798 + 3.24601i\,\mathrm{sign}t)t^2}. \tag{3.25}$$

This contour is shown in Fig. 6, along with the quadratic and exact contours. The shape of the integrand along this contour is again very similar to that shown in Fig. 4 for the quadratic contour. The differences are noticeable only on a logarithmic scale, shown side by side in Fig. 7. In Fig. 8, we show for comparison the integrand along the exact contour of stationary phase running through the stationary point, as computed using the differential equation. The difference in shape is due to the different parametrization of the curve (for the exact contour, we take the imaginary part to simply be t). The principal improvement along the exact contour is the complete absence of the imaginary part.

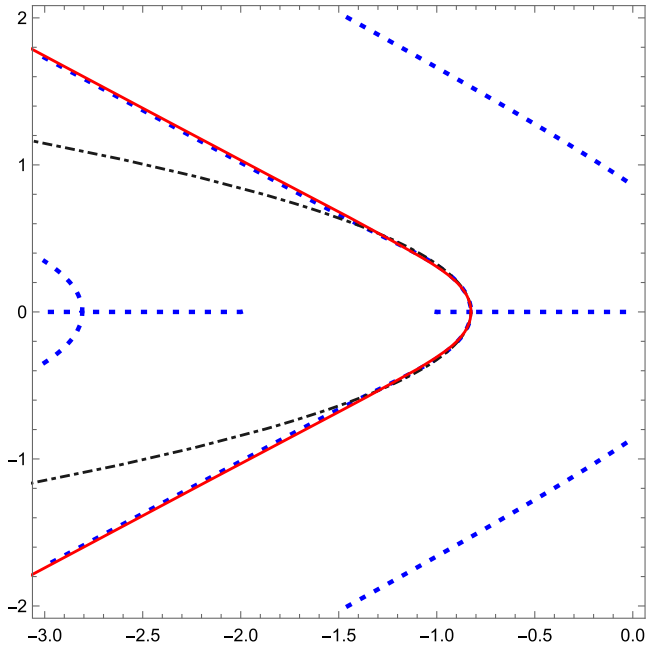

FIG. 6. The quadratic (dot-dashed dark gray) and [3/2] Padé (solid red) contours for the integrand $F_1(z,s)$ of Eq. (2.2) with $s=-\frac{1}{20}$, shown against the exact contours of zero phase (dotted blue).

We can of course construct higher-order curves, to serve as closer approximations to the true stationary-phase contour in the small-t region, if desired. For example, a quartic contour would be given by

$$z_4(t) = z_s + it + c_2t^2 + g_4t^4, \tag{3.26}$$

where

$$g_4 = -\frac{F^{(5)}(z_s)}{120F''(z_s)} + \frac{F^{(4)}(z_s)F^{(3)}(z_s)}{36(F''(z_s))^2} - \frac{1}{72}\left(\frac{F^{(3)}(z_s)}{F''(z_s)}\right)^3. \tag{3.27}$$

The formula for g_4 is obtained by requiring that the imaginary part of $F(z(t))$ vanish to $\mathcal{O}(t^5)$; in the Euclidean region, it will then automatically be real to $\mathcal{O}(t^6)$.

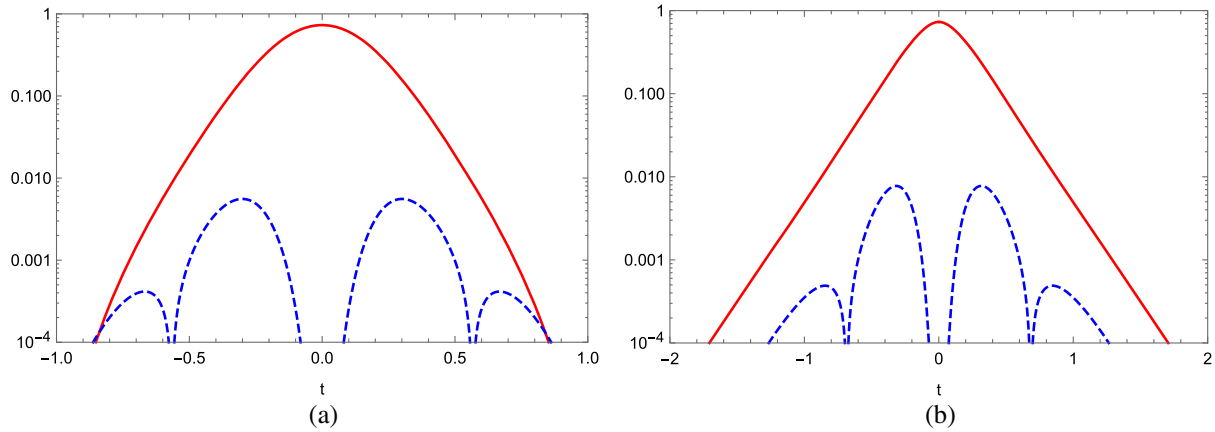

FIG. 7. The absolute values of the real (red) and imaginary (dashed blue) parts of the integrand $F_1(z,s)$ of Eq. (2.2) for $s=-\frac{1}{20}$ on (a) the quadratic contour of Eq. (3.7) (b) the Padé contour of Eq. (3.25).

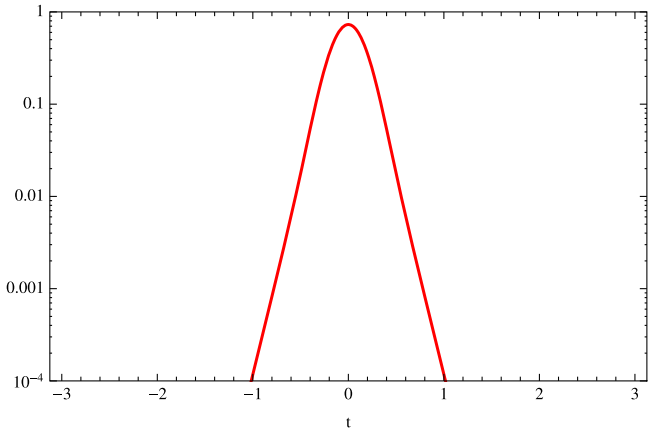

FIG. 8. The absolute values of the real (red) and imaginary (dashed blue) parts of the integrand $F_1(z,s)$ of Eq. (2.2) for $s = -\frac{1}{20}$ on the exact contour of stationary phase.

IV. MATCHING TO ASYMPTOTIC FORMS

We are interested in one-dimensional Mellin-Barnes integrals that arise from Feynman integrals with massive propagators. Labeling the integration variable of each Mellin-Barnes integral by z, the integrands contain gamma functions and their derivatives, with arguments of the form $n \pm z$ and $n \pm 2z$, where n is an integer (positive, negative, or zero). In general, the integrand is a sum of terms, where each term is a pure product of gamma functions, their derivatives, and inverses of gamma functions. Let us focus on each term separately, or equivalently restrict attention to integrands of the form

$$(-s)^{-z} \frac{\prod_{j\in\text{numer}}\Gamma(a_j + n_j z)\prod_{j\in\text{numer}}\psi^{(d_j)}(b_j + m_j z)}{\prod_{j\in\text{denom}}\Gamma(a_j + n_j z)}. \tag{4.1}$$

This makes it possible to write down general formulae for the asymptotic behavior of the integrand, and the corresponding parameters governing the contours of stationary phase.

The difference of numerator and denominator gamma function arguments is independent of z,

$$\frac{d}{dz}\left[\sum_{\substack{\text{numer}\\ \Gamma\text{s}}}\text{argument}\,(z) - \sum_{\substack{\text{denom}\\ \Gamma\text{s}}}\text{argument}\,(z)\right] = 0. \tag{4.2}$$

Denoting the coefficient of z in the argument to the jth gamma function by n_j, as in Eq. (4.1), we can rewrite this identity as

$$\sum_{\substack{\text{numer}\\ \Gamma\text{s}}} n_j - \sum_{\substack{\text{denom}\\ \Gamma\text{s}}} n_j = 0. \tag{4.3}$$

We can use this feature to derive a formula for the critical parameter s_0, as well as for the behavior of the integrand at large z. Considering only the exponential factors in the asymptotic form for the gamma function (3.8), we see that the gamma function factors in the integrand (or a single term if the integrand is a sum of terms) behave for large z (away from the real axis) as

$$\begin{aligned}
&\exp\left[-\left(\sum_{j\in\substack{\text{numer}\\ \Gamma\text{s}}} n_j - \sum_{j\in\substack{\text{denom}\\ \Gamma\text{s}}} n_j\right) z\right] \\
&\quad\times \exp\left[\left(\sum_{j\in\substack{\text{numer}\\ \Gamma\text{s}}} n_j - \sum_{j\in\substack{\text{denom}\\ \Gamma\text{s}}} n_j\right) z\ln z\right] \\
&\quad\times \exp\left[\left(\sum_{j\in\substack{\text{numer}\\ \Gamma\text{s}}} n_j \ln|n_j| - \sum_{j\in\substack{\text{denom}\\ \Gamma\text{s}}} n_j \ln|n_j|\right) z\right] \\
&\quad\times \exp\left[\left(\sum_{j\in\substack{\text{numer}\\ \Gamma\text{s}}} n_j \ln(\text{sign}\, n_j - i\delta\,\text{sign}\,\text{Im}\, z)\right.\right. \\
&\qquad\left.\left. - \sum_{j\in\substack{\text{denom}\\ \Gamma\text{s}}} n_j \ln(\text{sign}\, n_j - i\delta\,\text{sign}\,\text{Im}\, z)\right) z\right],
\end{aligned} \tag{4.4}$$

where we drop overall constants. Using the above identity (4.3), this asymptotic form simplifies to

$$\begin{aligned}
&\exp\left[\left(\sum_{j\in\substack{\text{numer}\\ \Gamma\text{s}}} n_j \ln|n_j| - \sum_{j\in\substack{\text{denom}\\ \Gamma\text{s}}} n_j \ln|n_j|\right) z\right] \\
&\quad\times \exp\left[\left(\sum_{j\in\substack{\text{numer}\\ \Gamma\text{s}}|n_j<0} |n_j| - \sum_{j\in\substack{\text{denom}\\ \Gamma\text{s}}|n_j<0} |n_j|\right) i\pi z\,\text{sign}\,\text{Im}\, z\right].
\end{aligned} \tag{4.5}$$

The exponential part of the integrand's behavior is not modified by possible polygamma function factors, as these have logarithmic or power-like asymptotic behavior. The critical value of s, which determines in which direction the contour must bend in order to ensure convergence as the contour parameter $t \to \pm\infty$, is then given by

$$s_0 = \frac{\prod_{j\in\substack{\text{numer}\\ \Gamma\text{s}}}|n_j|^{n_j}}{\prod_{j\in\substack{\text{denom}\\ \Gamma\text{s}}}|n_j|^{n_j}}. \tag{4.6}$$

Assuming the argument s appears in the integrand as $(-s)^{-z}$, for $|s| < s_0$, the contour must bend left, towards negative values of $\text{Re}\, z$, while for $|s| > s_0$, it must bend right, towards positive values of $\text{Re}\, z$. The integer offset in the argument of the jth gamma function (that is, the integer value obtained by setting $z = 0$) in Eq. (4.1) is denoted by a_j. It will be convenient to define

$$N_- \equiv \sum_{j\in\substack{\text{numer}\\ \Gamma\text{s}}|n_j<0} |n_j| - \sum_{j\in\substack{\text{denom}\\ \Gamma\text{s}}|n_j<0} |n_j|, \tag{4.7}$$

$$S_+ \equiv \sum_{j\in\substack{\text{numer}\\ \Gamma\text{s}}|n_j>0} 1 - \sum_{j\in\substack{\text{denom}\\ \Gamma\text{s}}|n_j>0} 1, \tag{4.8}$$

$$S_- \equiv \sum_{j\in{}^{\text{numer}}_{\Gamma\text{s}}|n_j<0} 1 - \sum_{j\in{}^{\text{denom}}_{\Gamma\text{s}}|n_j<0} 1, \tag{4.9}$$

$$A_+ \equiv \sum_{j\in{}^{\text{numer}}_{\Gamma\text{s}}|n_j>0} a_j - \sum_{j\in{}^{\text{denom}}_{\Gamma\text{s}}|n_j>0} a_j, \tag{4.10}$$

and

$$A_- \equiv \sum_{j\in{}^{\text{numer}}_{\Gamma\text{s}}|n_j<0} a_j - \sum_{j\in{}^{\text{denom}}_{\Gamma\text{s}}|n_j<0} a_j. \tag{4.11}$$

[We do not need N_+, corresponding to $n_j > 0$, thanks to Eq. (4.3).] Denoting the number of derivatives of the jth polygamma function $\psi^{(d)}(z)$ (always in the numerator) by d_j, with m_j the coefficient of z in the argument let us also define

$$\begin{aligned} D_+^{(\psi)} &\equiv \sum_{j\in\psi\text{s}|m_j>0} d_j, \\ D_-^{(\psi)} &\equiv \sum_{j\in\psi\text{s}|m_j<0} d_j, \\ S^{(\psi)} &\equiv \sum_{j\in\psi\text{s}} 1, \end{aligned} \tag{4.12}$$

where the sums are not taken over the basic polygamma function $\psi(z)$ but only over its derivatives $\psi^{(d)}(z)$.

Using them, we can express the remaining square-root factors in Eq. (3.8) in a compact form, so that the asymptotic behavior of the integrand as a whole is

$$\begin{aligned} F &\sim \text{const}\left(\frac{s_0}{-s}\right)^z e^{i\pi z N_-\text{sign Im}\, z}(-1)^{D_+^{(\psi)}+D_-^{(\psi)}+S^{(\psi)}} z^{-S_+/2+A_+-D_+^{(\psi)}}(-z)^{-S_-/2+A_--D_-^{(\psi)}} \\ &= \text{const}\left(\frac{s_0}{-s}\right)^z e^{i\pi z N_-\text{sign Im}\, z}(-1+i\delta\,\text{sign Im}\, z)^{-S_+/2+A_++D_-^{(\psi)}+S^{(\psi)}}(-z)^{-S_+/2-S_-/2+A_++A_--D_+^{(\psi)}-D_-^{(\psi)}}, \end{aligned} \tag{4.13}$$

where we have rewritten $z^a = [(-1+i\delta\,\text{sign Im}\, z)(-z)]^a$, and used the fact that $D_\pm^{(\psi)}$ and $S^{(\psi)}$ are integers, along with $(-1)^n = (-1+i\delta\,\text{sign Im}\, z)^n$ for integer n.

The phase of this expression is

$$\begin{aligned} \arg F = \Bigg[&\text{Im}\, z \ln\left(\frac{s_0}{-s}\right) + \pi\,\text{Re}\, z N_-\text{sign Im}\, z - \frac{\pi}{2}((S_+ - 2A_+ - 2D_-^{(\psi)} - 2S^{(\psi)}) \bmod 4)\text{sign Im}\, z \\ &+ (-S_+/2 - S_-/2 + A_+ + A_- - D_+^{(\psi)} - D_-^{(\psi)})\arg(-z)\Bigg] \bmod 2\pi, \end{aligned} \tag{4.14}$$

generalizing Eq. (3.12). (Here, n mod m is understood to mean $(\text{sign}n)(|n| \bmod m)$, and the mod 2π is understood to reduce the variable to the range $(-\pi, \pi]$.)

Substituting the form in Eq. (3.13), expanding in t, and setting the coefficient of the $\mathcal{O}(t)$ term to zero, and that of the $\mathcal{O}(t^0)$ term to ϕ_s allows us to obtain general formulae for θ_∞ and z_∞,

$$\begin{aligned} \theta_\infty &= \text{atan}\left[\frac{1}{\pi N_-}\ln\left(\frac{s_0}{-s}\right)\right], \qquad N_- \neq 0, \\ \theta_\infty &= \text{sign}\,\ln\left(\frac{s_0}{-s}\right)\frac{\pi}{2}, \qquad N_- = 0, \\ z_\infty &= \frac{\phi_s \text{sign Im}\, z_s}{\pi N_-} + \frac{(S_+ - 2A_+ - 2D_-^{(\psi)} - 2S^{(\psi)}) \bmod 4}{2N_-} \\ &\quad - \frac{1}{N_-\pi}\left[(A_+ + A_- - S_+/2 - S_-/2 - D_+^{(\psi)} - D_-^{(\psi)})\left(\theta_\infty - \frac{\pi}{2}\right) \bmod 2\pi\right], \qquad N_- \neq 0, \\ z_0^{(+\infty)} &= i\left|\frac{\phi_s}{\ln(s_0/(-s))} + \frac{\pi}{2}\frac{(S_+ - 2A_+ - 2D_-^{(\psi)} - 2S^{(\psi)}) \bmod 4}{\ln(s_0/(-s))}\right. \\ &\quad \left. - \frac{1}{\ln(s_0/(-s))}\left[(A_+ + A_- - S_+/2 - S_-/2 - D_+^{(\psi)} - D_-^{(\psi)})\left(\theta_\infty - \frac{\pi}{2}\right) \bmod 2\pi\right]\right|, \qquad N_- = 0, \end{aligned} \tag{4.15}$$

valid in the Euclidean region (for $s \neq -s_0$). Factors of the polygamma $\psi(z)$ (with no derivatives) will correct the large-t behavior by terms of $\mathcal{O}(1/\ln t)$, which are noticeable visually on contour plots, but have no practical importance in computing the integral. In the generic case, $\phi_s = 0$ or π, but the formulas are valid more generally; we take sign Im 0 to be 1. (We have implicitly assumed that $\theta_\infty \in [-\frac{\pi}{2}, \frac{\pi}{2}]$ in deriving these results.)

In these formulas, $\phi_s = 0$ if $F(z_s) \geq 0$, while $\phi_s = \pi$ if $F(z_s) < 0$. For $N_- \neq 0$, the value for z_∞ may be shifted by an integer multiple of $2/N_-$. (A good heuristic is to choose z_∞ in the original interval of interest.) For $N_- = 0$, the asymptotes are parallel to the real axis, and so we cannot take z_∞ to be real; we must replace z_∞ by $z_0^{(+\infty)}\Theta(t) - z_0^{(+\infty)}\Theta(-t)$ in Eq. (3.18), where $\Theta(t)$ is the usual Heaviside step function. For this value of N_-, we can shift $z_0^{(+\infty)}$ by a multiple of $2\pi i/\ln(s_0/(-s))$. [In some cases, it may be appropriate to shift by half this amount. A good heuristic here is to choose $z_0^{(+\infty)}$ to lie in the interval $i[1/c_2 - \pi/\ln(s_0/(-s)), 1/c_2 + \pi/\ln(s_0/(-s))]$, where c_2 is the quadratic coefficient given in Eq. (3.6).]

These expressions for θ_∞ and $z_0^{(+\infty)}$, along with that for c_2 given in Eq. (3.6), allow us to compute the coefficients of the Padé approximation (3.16) in the Euclidean region via Eqs. (3.17)–(3.24), (4.7)–(4.12), and (4.15) for a generic one-dimensional Mellin-Barnes integrand arising from Feynman diagrams.

V. OTHER INTEGRANDS

The integrands in which we are interested have poles at most integer values; may have zeros or poles at half-integer values, and may have additional zeros along the real axis. The integrand considered in the previous section is generic, but its properties are not universal: it has poles at every integer value, and zeros at every positive half-integer value. At the ends of each integer interval $(n, n+1)$ with $n < 0$, it blows up with the same sign, so that each integer interval contains an extremum. This is shown in Fig. 9, with the aid of a function designed to compress the vertical scale,

$$\operatorname*{sln}_m x \equiv \operatorname{sign} x \ln(1 + |x| e^m). \tag{5.1}$$

For purposes of drawing contours of stationary phase and approximations thereto, it is not essential that the extremum be a minimum, of course; if it is a local maximum, one can convert it to a minimum by considering the negative of the integrand.

What other classes of integrands should we consider? In this section, we discuss a few less-generic but possible forms of integrands, and discuss how the contours in the previous section are modified.

A. Intervals without extrema

Not all integrands that arise in calculations of interest share the nice feature of the one in Eq. (2.2), namely that the integrand blows up with the same sign at both ends of for integer (or half-integer) intervals of interest. For example, consider the integrand obtained by multiplying that of Eq. (2.2) by a polygamma function,

$$F_2(z, s) = (-s)^{-z} \frac{\Gamma^3(-z)\Gamma(1+z)\psi(-2z)}{\Gamma(-2z)}. \tag{5.2}$$

If we are interested in deforming the contour passing through $\operatorname{Re} z = -\frac{1}{2}$ slightly to obtain a contour of stationary phase, we see from Fig. 10 that this is not possible because the integrand has no extremum in the interval $(-1, 0)$. Indeed, the lone stationary point on the real axis is replaced by a complex-conjugate pair of stationary points. In addition, the function necessarily has at least one zero in the interval. These features require a substantial modification of the contours discussed in the previous section, a point to which we shall return in Sec. VII.

In the case of F_2, however, we can simply shift the contour to the interval $(-2, -1)$. We pick up an additional contribution from the residue at -1, so that

$$\begin{aligned} I_2(s) &= \frac{1}{2\pi i} \int_{c_0 - i\infty}^{c_0 + i\infty} dz F_2(z, s) \\ &= (-1 + \gamma_E) + s \frac{1}{2\pi i} \int_{c_1 - i\infty}^{c_1 + i\infty} dz F_2(z, s), \end{aligned} \tag{5.3}$$

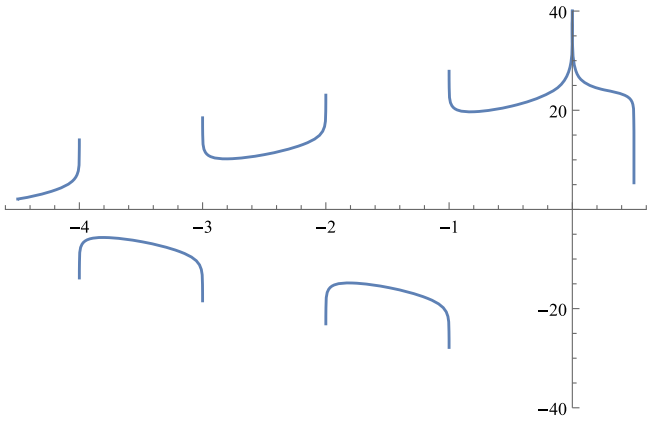

FIG. 9. The behavior of the integrand $F_1(z, s)$ in Eq. (2.2), along the real axis. The plot displays sln_{20}(integrand), with $s = -\frac{1}{20}$.

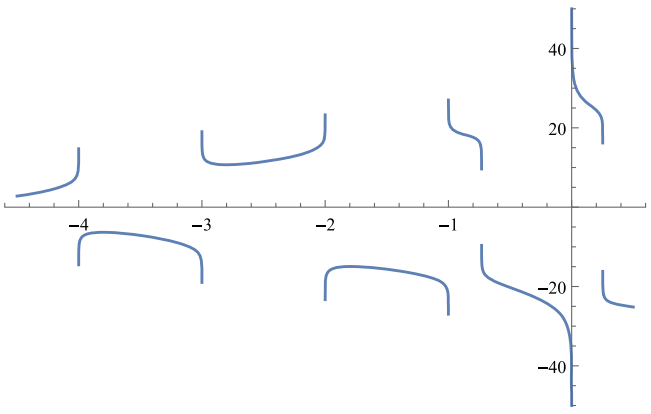

FIG. 10. The behavior of the integrand $F_2(z, s)$ of Eq. (5.2), along the real axis. The plot displays sln_{20}(integrand), with $s = -\frac{1}{20}$.

where $c_1 = -3/2$. We can apply the approach of the previous section to the second integral, as its integrand does have a stationary point on the real axis in the new interval.

It can happen that there is *no* interval which has a local extremum. As mentioned above, we will return to a consideration of such integrands in Sec. VII.

B. Wrong-direction quadratic contour

As discussed in the previous section, we can use the asymptotic expansion for the gamma function in order to study the large-z behavior of the integrand. For the integrand $F_1(z,s)$ in Eq. (2.2), we found (3.10) that it behaves like

$$\text{const}\, 4^z(-s)^{-z}\frac{(-1+i\delta\,\text{sign}\,\text{Im}\,z)^{z+1/2}}{\sqrt{-z}}. \tag{5.4}$$

The factor $(-1+i\delta\,\text{sign}\,\text{Im}\,z)^z$ is convergent as $z\to\infty$ both above and below the real axis, independently of the sign of the real part of z. The first two factors do however care which direction the contour goes. For $-4<s<0$, they require us to close the contour to the left; otherwise these factors will blow up when $\text{Re}\,z\to-\infty$. Similarly, for $s<-4$, they require us to close the contour to the right. The quadratic contour (3.7), for $s=-\frac{1}{20}$, has the desired form, veering away from the imaginary axis to the left. This is also true by construction, of course, for the $[3/2]$ Padé contour (3.25). However, the plain quadratic contour does not always have this property. Consider the following integrand:

$$F_3(z,s)=(-s)^{-z}\frac{\Gamma^3(-z)\Gamma(1+z)\psi(-z)}{\Gamma(-2z)}. \tag{5.5}$$

The various quadratic approximations along with the exact contours of zero phase are shown in Fig. 11 for $s=-20$. In this case, the pure quadratic contour veers to the left, whereas convergence requires the contour to veer to the right.

In contrast, the form of the $[3/2]$ Padé contour (3.16) requires no modification; it heads off in the correct direction, thereby solving the problem with the simple quadratic contour. This is one of the reasons the use of the asymptotic contour is helpful, even though the contributions to the integral from the asymptotic region are exponentially small. In this particular case, the quartic contour of Eq. (3.26) would also head off towards the correct side of the complex plane; but one can always find examples where a given fixed-order contour heads off in the wrong direction. All three contours are shown in Fig. 11. (The Padé contour shown has its z_∞ intercept shifted to the interval $(-2,-1)$, but this does not affect the overall qualitative features compared to having it in the interval $(-1,0)$.)

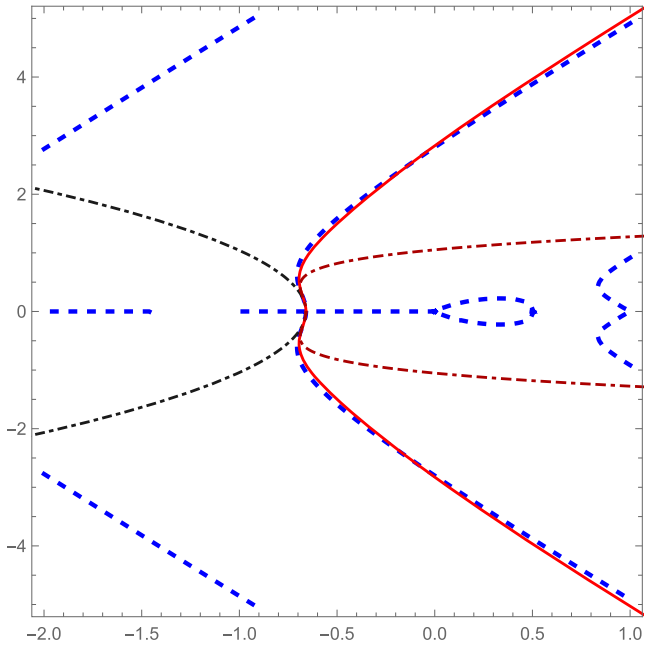

FIG. 11. The quadratic (dot-dashed dark gray), $[3/2]$ Padé (solid red), and quartic (dot double-dashed dark red) contours for the integrand $F_3(z,s)$ of Eq. (5.5) with $s=-20$, shown against the exact contours of zero phase (dotted blue).

C. Vanishing curvature

The formula (3.6) for the coefficient of the quadratic term in the contour assumes that the second derivative at the local extremum does not vanish. While this is typically true, one encounters examples where it is false. Such an example is given by the following integrand:

$$F_4(z,s)=(-s)^{-z}\frac{\Gamma^3(-z)\Gamma(1+z)\psi^4(1-z)}{\Gamma(-2z)}. \tag{5.6}$$

In general, if the integrand blows up with the same sign at both ends of a pole-free interval (ensuring that there is an absolute extremum on the interval), and the second derivative vanishes at a given local extremum, there are two possibilities: either the third derivative also vanishes, or it is nonvanishing. In the latter case, there is then another, lower minimum (higher maximum), which is what we should pick as the base point for the contour. If the third derivative also vanishes, we must modify our approach. In the above example, the integrand vanishes at the extremum in the interval $(-1,0)$, which is in fact the likeliest way for a single-term Mellin-Barnes integrand of the type we are considering to have a vanishing second derivative. We could again handle it by shifting to a different interval along the negative real axis, where the extremum will be quadratic. Evaluating it with a contour in the interval $(-1,0)$ is also possible, but requires the use of techniques of the same sort considered in Sec. VII for integrands without extrema on the real axis.

D. Flat asymptotes

In the examples considered above, $N_- \neq 0$. In contrast,

$$F_5(z,s) = (-s)^{-z} \frac{\Gamma^3(-z)\Gamma(1+z)}{\Gamma(-2z)\Gamma(1-z)\Gamma(2+z)} \tag{5.7}$$

has $N_- = 0$. As a result, the asymptotes of stationary-phase contours will be parallel to the real axis. The formulas derived in previous sections hold for this case, but one must use the special forms for $N_- = 0$ in Eq. (4.15). The quadratic and [3/2] Padé contours for $s = -\frac{1}{20}$ are shown in Fig. 12; and the behavior of the integrand along the Padé contour is shown in Fig. 13(a). It has generic behavior, in spite of the special case needed for the contour. In Fig. 13(b), we show the behavior along the exact contour of stationary phase, computed using the differential-equation approach discussed in Sec. II; in the latter, the imaginary part of the contour is again chosen to be t. The absence of oscillations in the real part along the Padé contour, together with the imaginary part being essentially zero in both parts of the figure attest to the good quality of approximation it furnishes.

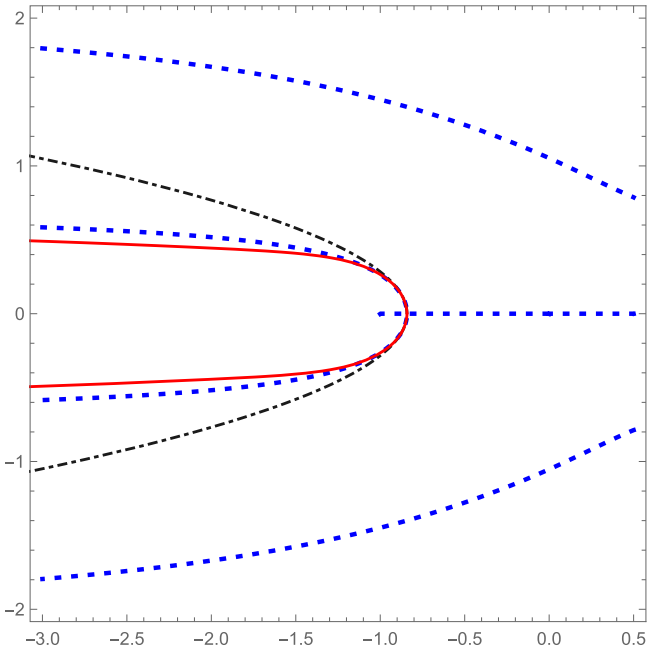

FIG. 12. The quadratic (dot-dashed dark gray) and [3/2] Padé (solid red) contours for the integrand $F_5(z,s)$ of Eq. (5.7), with $s = -\frac{1}{20}$, shown along with the exact contours of stationary phase (dotted blue).

E. Closed contours

The exact contour of stationary phase passing through a given saddle point on the real axis may be closed: it may end at a zero, or at another saddle point. (Lines of steepest *ascent* can also run into poles.) The following integrand provides an example:

$$F_6(z,s) = (-s)^{-z} \frac{\Gamma^4(-z)\Gamma(1+2z)}{\Gamma^2(-2z)\Gamma^2(1+z)}. \tag{5.8}$$

For $s = -\frac{1}{8}$, the integrand has a saddle point at

$$z_s = -0.408258. \tag{5.9}$$

For this integrand, saddle points come in pairs in each half-interval $(-n-1/2, -n)$, $n \in \mathbb{Z}_+$, leading to a sequence of closed contours for small z, as shown in Fig. 14(a). Contours end on the rightmost of each pair, and begin at the leftmost. As n grows, the elements of the pairs approach each other, and eventually move off the real axis. At that point, we do get a single stationary-phase contour enclosing all remaining poles. This is illustrated for $F_6(z, -\frac{1}{8})$ in Fig. 14(b) (for $s = -\frac{1}{20}$, this only occurs for $z \gg 10^{12}$). However, from a practical point of view, using the exact

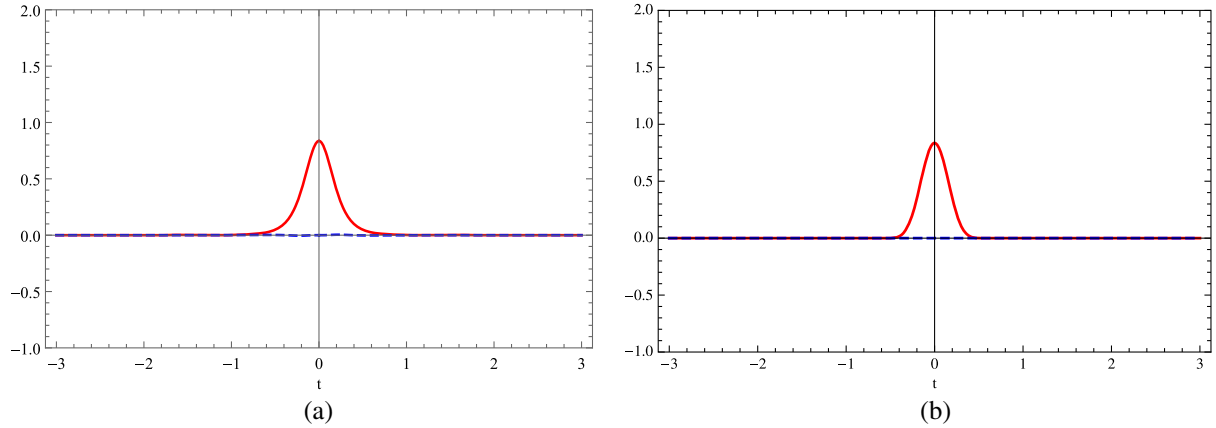

FIG. 13. The real (red) and imaginary (dashed blue) parts of the integrand $F_5(z,s)$ of Eq. (5.7) for $s = -\frac{1}{20}$ along (a) the [3/2] Padé contour (b) the exact contour.

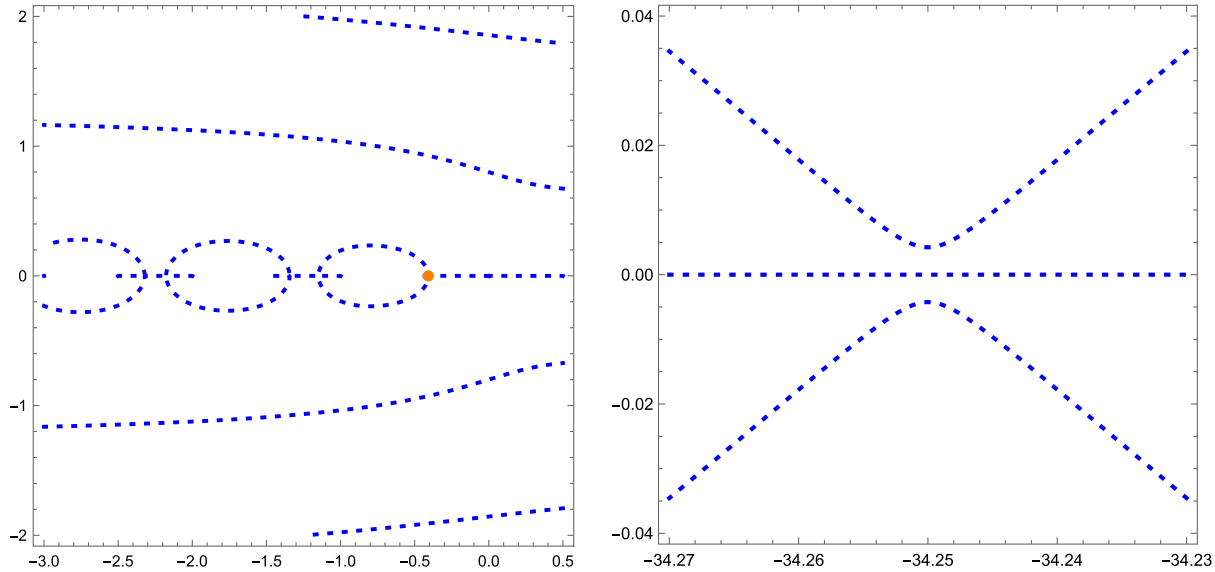

FIG. 14. Exact contours (dotted blue) of stationary phase for the integrand $F_6(z,s)$ of Eq. (5.8), with $s=-\frac{1}{8}$ (a) at small $|z|$ (b) at larger $|z|$. The saddle point in the interval $(-\frac{1}{2},0)$ is also shown (orange dot).

contour (or ensemble of contours) is pointless, as it would amount to summing over residues for the bulk of the contribution. One might as well compute the residues analytically and sum over them directly. In contrast, the approximate $[3/2]$ Padé contour interpolates between the stationary-phase contour at the beginning, and the asymptotic contour (which in this case is parallel to the real axis). The Padé contour obtained using the forms described in Secs. III and IV is shown in Fig. 15, and the value of the integrand along this contour is shown in Fig. 16. It necessarily has oscillations, but the overall fall-off, and hence the expected convergence of integration, is rapid.

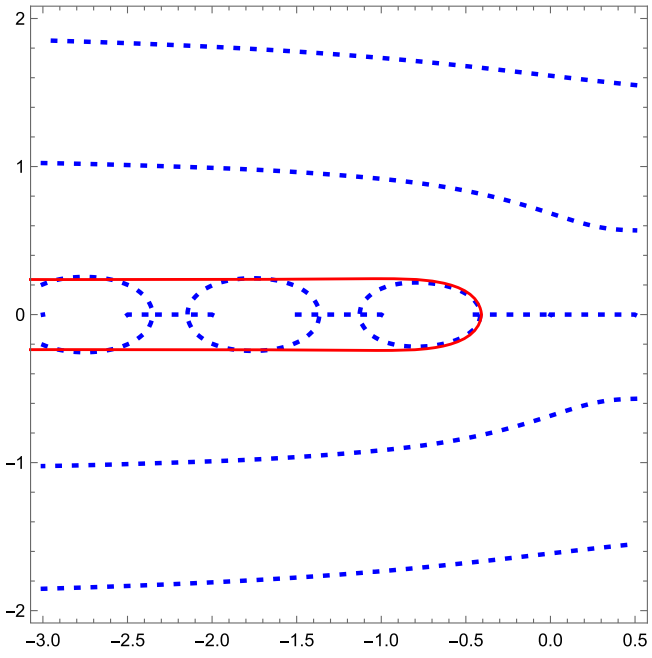

FIG. 15. The $[3/2]$ Padé (solid red) contour for the integrand $F_6(z,s)$ of Eq. (5.8) with $s=-\frac{1}{8}$ for $s=-\frac{1}{20}$, shown against the exact contours of zero phase for the integrand (dotted blue).

VI. MINKOWSKI INTEGRALS

A. Below threshold

We now turn our attention to the evaluation of integrals in the Minkowski region. In this region, the naive textbook and MB contours yield integrals which are often only

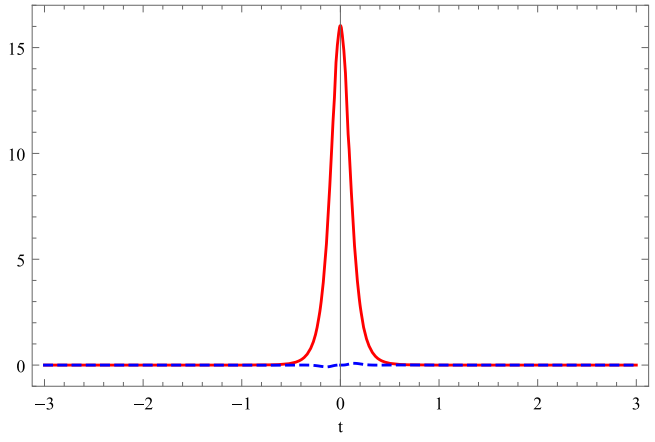

FIG. 16. The real (red) and imaginary (dashed blue) parts of the integrand $F_6(z,s)$ of Eq. (5.8) for $s=-\frac{1}{8}$ along the $[3/2]$ Padé approximation to the contour of zero phase.

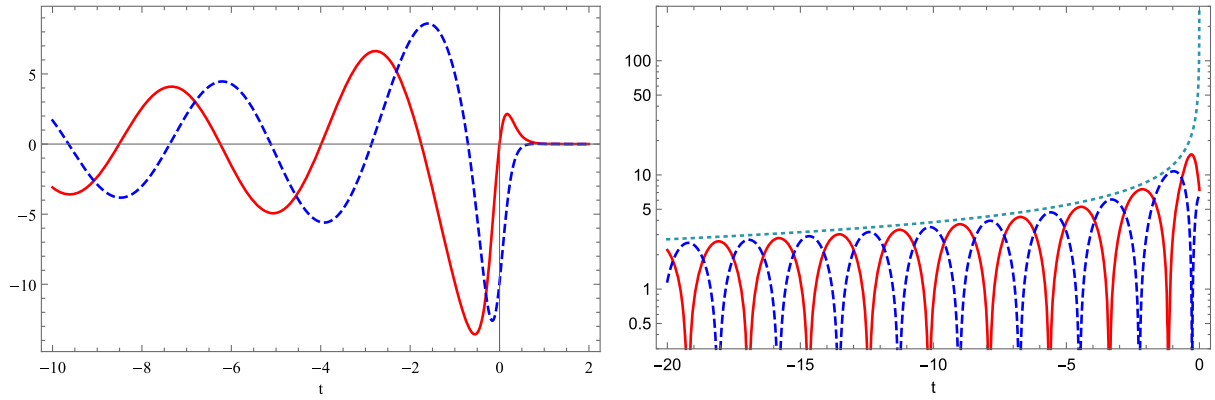

FIG. 17. The real (red) and imaginary (dashed blue) parts of the integrand $F_1(z, s)$ of Eq. (2.2), for $s = 1 + i\delta$, along the MB contour $\mathrm{Re}\, z = -\frac{1}{2}$. The parts are shown on a linear scale in (a), and their absolute values on a log scale in (b). The dotted (dark turquoise) curve in (b) is a curve decreasing as $t^{-1/2}$.

conditionally (but not absolutely) convergent, and hence do not readily converge numerically. In some cases, special numerical techniques can be brought to bear, but for most, we need to find a different contour.

We start with the example of Eq. (2.1), but now for $s > 0$. The integrand now has an imaginary part even for real z, and correspondingly, the integral may also have an imaginary part. The oscillations along the naive contour $\mathrm{Re}\, z = -\frac{1}{2}$ are only slowly damped, as shown in Fig. 17 for $s = 1 + i\delta$ (with $\delta = 10^{-10}$). This value is below the threshold at $s = 4$, but straightforward numerical integration already fails to converge.

To find a better contour, we again seek a contour of stationary phase. Unlike the Euclidean case, however, this phase will not be zero; nor will the corresponding saddle point sit on the real axis. We seek contours which pass from infinity (with large negative imaginary part of z) through the saddle point and back to infinity (with large positive imaginary part of z). Even below threshold, we must add an infinitesimal imaginary part to the parameter s in order to specify a contour; we will take it to be positive. The integrand of Eq. (2.2) has another feature which is generic, but complicates the analysis: it vanishes for positive half-integer values of z. Zeros of the integrand complicate the analysis because lines of stationary phase (and hence contours) can (and typically do) end on them; this would force us to look for half-contours, combining them with discontinuous derivatives at the zero to obtain full contours. We will treat that case in Sec. VII.

Our first task is to find the saddle points, that is the points where the derivative of the integrand vanishes. When using MATHEMATICA to do this, it is best to seek minima of the absolute value of the derivative, rather than roots of the equations, as this approach is more stable. It is in any case helpful to bound the search to a strip consisting of the imaginary extension of the original integer interval containing the naive contour.

For $\mathrm{Re}\, z < 0$, we find a single series of solutions,

$$z = -0.78932 - 0.174532i, \quad -1.78841 - 0.212806i, \ldots \tag{6.1}$$

For $\mathrm{Re}\, z > 0$, we find two series of solutions, one above the real axis, the other below:

$$z = 0.313742 - 0.476771i, \quad 0.482908 + 0.17074i; \\ 1.25952 - 0.452846i, \quad 1.47558 + 0.171388i; \ldots \tag{6.2}$$

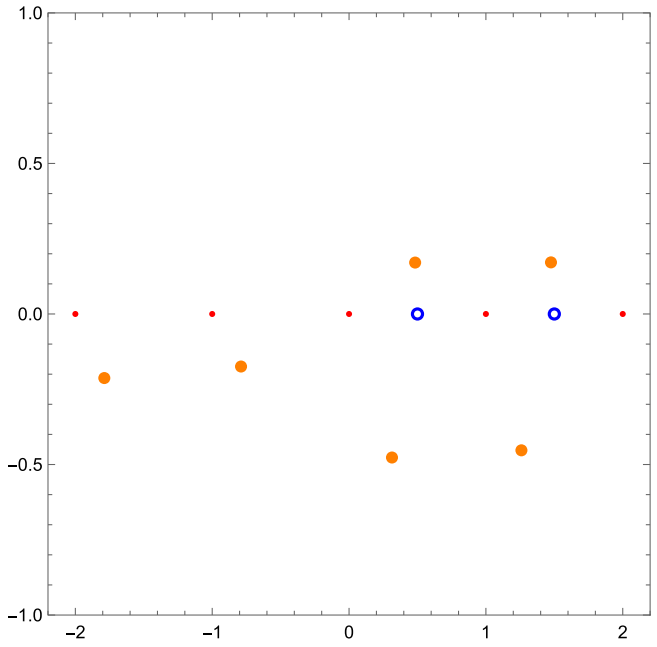

FIG. 18. The saddle points (large orange dots), poles (small red dots), and zeros (blue circles) of the integrand of Eq. (2.2) for $s = 1 + i\delta$.

These solutions, along with the poles and zeros of the integrand, are shown in Fig. 18. The doubling of solutions for positive $\mathrm{Re}\, z$ is directly related to the presence of nearby real zeros at positive half-integer values. These are stationary points which would require patching together two contours of stationary phase which would meet at the associated zero. The solutions for $\mathrm{Re}\, z < 0$, in contrast, are associated with a single contour running from infinity in to the stationary point, and then back out to infinity. Let us, therefore, set aside the solutions for $\mathrm{Re}\, z > 0$, and base a contour on the first solution in the first set, $z_s = -0.78932 - 0.174532i$. The phase at this point is $e^{i\phi_s}$, with $\phi_s = -2.29000$.

Let us again begin by finding a linear approximation to the contour of stationary phase, given by the tangent to the contour at the saddle point. Writing

$$z(t) = z_s + e^{i\theta_s}(x(t) + iy(t)), \tag{6.3}$$

where $x(0) = y(0) = 0$, without loss of generality we can again take $x'(0) = 0$ and $y'(0) = 1$. Because z_s is a saddle point, the expansion of the integrand F around $t = 0$ has no linear term,

$$F = F(z_s) - \frac{1}{2}F''(z_s)e^{2i\theta_s}t^2. \tag{6.4}$$

We require the integrand to be of stationary phase along this contour,

$$-\frac{1}{2}\mathrm{Im}\left[\frac{F''(z_s)e^{2i\theta_s}}{F(z_s)}\right] = 0. \tag{6.5}$$

We can solve for θ_s,

$$\theta_s = -\frac{1}{2}\arg\left[\frac{F''(z_s)}{F(z_s)}\right]. \tag{6.6}$$

Equation (6.5) also allows for solutions shifted by $\pi n/2$. Shifting by π is harmless; it just amounts to exchanging $t \leftrightarrow -t$ in Eq. (6.3). To fix an orientation, we can adopt the convention that θ_s should lie in the interval $[-\frac{\pi}{2}, \frac{\pi}{2}]$. In order to select between θ_s and $\theta_s + \pi/2$, we should pick the direction in which the absolute value of the function decreases in magnitude. (This is equivalent to requiring that $\mathrm{Re}[e^{2i\theta_s}F''(z_s)/F(z_s)]$ be negative.)

In the example at hand, this linear contour has the form

$$z_t(t) = -0.78932 - 0.174532i + (0.504583 + 0.863363i)t. \tag{6.7}$$

It is shown in Fig. 19. The real and imaginary parts of the integrand along this contour, with the phase $e^{i\phi_s}$ at the saddle point divided out, are shown in Fig. 20; although they still oscillate, the oscillations are damped, and the integral can be computed numerically. This contour is an example of the kind of contour proposed by Freitas and Huang [46], though their approach does not use the criterion used here to determine θ_s. (In any case, the solution given here for the tangent contour does not give a numerically stable integral for all values of s or all integrands.)

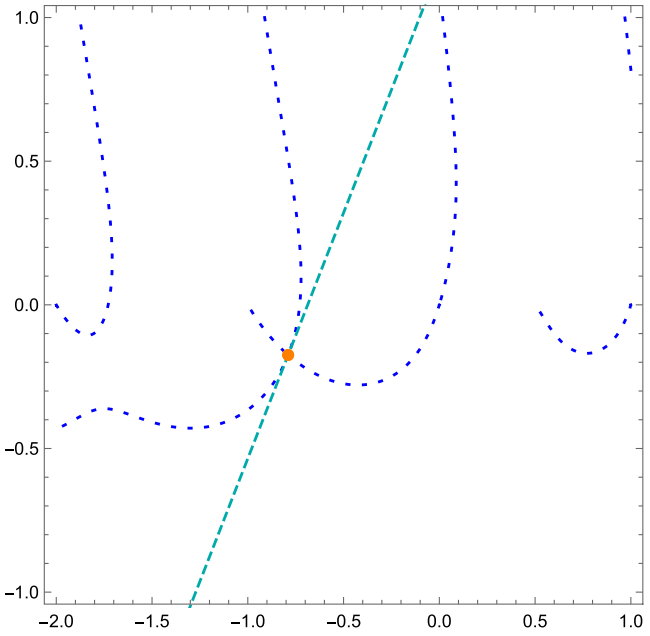

FIG. 19. Contours of constant phase $e^{i\phi_s}$ (dotted blue) for the integrand $F_1(z, s)$ of Eq. (2.2) with $s = 1 + i\delta$. The saddle point is denoted by the large orange dot. The linear (tangent) approximation to the contour of stationary phase is the dashed (dark turquoise) line.

As in the Euclidean case, we can improve the contour further. It will be convenient to define an abbreviation,

$$D_n \equiv e^{in\theta_s}\frac{F^{(n)}(z_s)}{F(z_s)}. \tag{6.8}$$

Let us examine the stationary-phase equation resulting from expanding the integrand to one higher order,

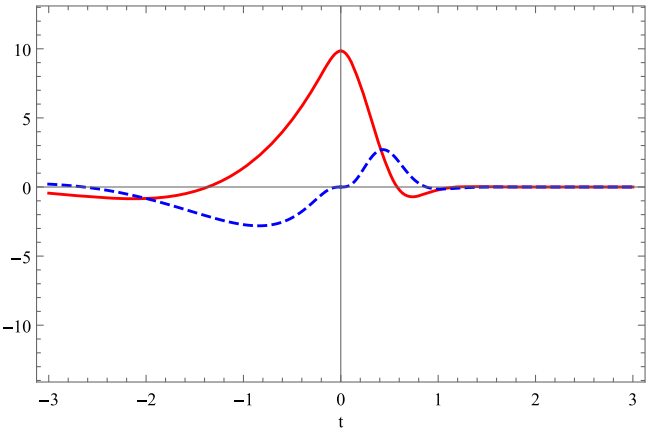

FIG. 20. The real (red) and imaginary (dashed blue) parts of the integrand $F_1(z, s)$ of Eq. (2.2) with $s = 1 + i\delta$, divided by the phase at the saddle point, along the linear contour of Eq. (6.7).

$$-\frac{1}{2}t^2\mathrm{Im}[D_2]-\frac{1}{6}t^3\mathrm{Re}[D_3] + \frac{1}{2}t^3\mathrm{Re}[D_2]x''(0)-\frac{1}{2}t^3\mathrm{Im}[D_2]y''(0)=0. \quad (6.9)$$

Using the solution to the lower-order equation (6.6), which forces D_2 to be real, we can simplify this equation to obtain

$$x''(0)=\frac{1}{3}\mathrm{Re}[D_3]/D_2. \quad (6.10)$$

so that

$$z_q(t)=z_s+e^{i\theta_s}(it+c_2t^2), \quad (6.11)$$

with c_2 set to $z_2\equiv x''(0)/2$. This generalizes Eq. (3.6) to the Minkowski region. In the example at hand, this would lead to the quadratic contour,

$$z_q(t)=(-0.78932-0.174532i) + (0.863363-0.504583i)(it-1.09478t^2). \quad (6.12)$$

Unlike the Euclidean case, this quadratic contour does not automatically make the phase stationary through $\mathcal{O}(t^4)$; setting the imaginary part of that order to zero, we find

$$y''(0)=\frac{\mathrm{Im}[D_4]}{4\mathrm{Re}[D_3]}-\frac{\mathrm{Im}[D_3]}{2D_2} \quad (6.13)$$

and set $c_2=x''(0)/2+iy''(0)/2$. In the example at hand, this leads to the quadratic contour,

$$z_q(t)=(-0.78932-0.174532i) + (0.863363-0.504583i) \times (it-(1.09478-0.026705i)t^2), \quad (6.14)$$

which is very similar to the one given in Eq. (6.12). The solution for $y''(0)$ depends on truncating the contour at the quadratic order; otherwise, $x^{(3)}(0)$ would also appear in the equation.

For small t, both of these contours provide an excellent approximation to the true contour of steepest descent, and essentially eliminate oscillations in the integrand. They suffer from a problem, however, illustrated in Fig. 21: because the first is symmetric around a line inclined to the real axis, and the second nearly so, at large negative t they will cross the real axis, thus failing to include the contributions of the remaining series of poles at larger negative z. The numerical contributions of the corresponding residues are small, but this truncation is uncontrolled: no matter how many points we throw at the integration, we can never obtain the correct answer.

In order to solve this problem, we need to modify the behavior of the contour at larger t. One way of doing this is to match to the asymptotic form contour for large z. In this case, the two asymptotic regions, $t\to+\infty$ and $t\to-\infty$ are no longer complex conjugates, and so we will have two different angles, which we denote $\theta_{+\infty}$ and $\theta_{-\infty}$, respectively.

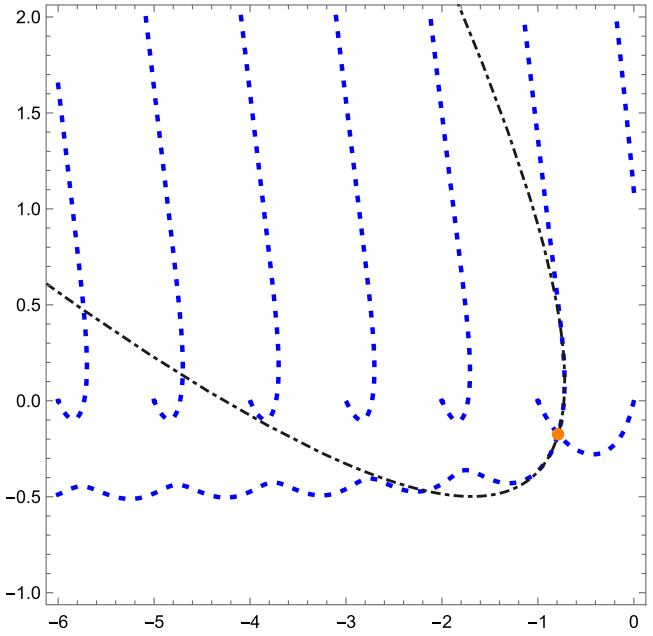

FIG. 21. The quadratic approximation (6.14) to the stationary-phase contour (solid red) for the integrand of Eq. (2.1) with $s=1+i\delta$. The exact contours of constant phase $e^{i\phi_s}$ are also shown (dotted blue). The saddle point is indicated by a large orange dot.

To find these angles, we generalize the discussion of the asymptotic form of the integrand in Sec. IV. The only difference is in the $(-s)^{-z}$ factor; the phase now comes from the real part of z as well as the imaginary part. We find an additional contribution to $\arg F$ beyond that given in Eq. (4.14), so that

$$\arg F=\mathrm{Im}\,z\ln\left|\frac{s_0}{-s}\right|+\pi\,\mathrm{Re}\,z(N_-\mathrm{sign}\,\mathrm{Im}\,z+\mathrm{sign}\,\mathrm{Im}\,s) -\frac{\pi}{2}((S_+-2A_+)\bmod 4)\mathrm{sign}\,\mathrm{Im}\,z + [(-S_+/2-S_-/2+A_++A_-)\arg(-z)]\bmod 2\pi. \quad (6.15)$$

Writing the large-z forms for the stationary-phase contour as follows,

$$z\overset{t\to+\infty}{\sim}z_\infty+ie^{i\theta_{+\infty}}t, \qquad t>0,$$
$$z\overset{t\to-\infty}{\sim}z_\infty+ie^{-i\theta_{-\infty}}t, \qquad t<0, \quad (6.16)$$

substituting into the asymptotic form for $\arg F$ and requiring the coefficient of t in the large-t expansion to vanish, leads to the following formulas for $\theta_{\pm\infty}$:

$$\begin{aligned}
\theta_{+\infty} &= \operatorname{atan}\left[\frac{1}{\pi(N_- + \operatorname{sign}\operatorname{Im} s)}\ln\left|\frac{s_0}{-s}\right|\right], && N_- \neq -\operatorname{sign}\operatorname{Im} s,\\
\theta_{+\infty} &= \operatorname{sign}\ln\left|\frac{s_0}{-s}\right|\frac{\pi}{2}, && N_- = -\operatorname{sign}\operatorname{Im} s,\\
\theta_{-\infty} &= \operatorname{atan}\left[\frac{1}{\pi(N_- - \operatorname{sign}\operatorname{Im} s)}\ln\left|\frac{s_0}{-s}\right|\right], && N_- \neq \operatorname{sign}\operatorname{Im} s,\\
\theta_{-\infty} &= \operatorname{sign}\ln\left|\frac{s_0}{-s}\right|\frac{\pi}{2}, && N_- = \operatorname{sign}\operatorname{Im} s.
\end{aligned} \tag{6.17}$$

These expressions reduce to the Euclidean results (4.15) so long as we take $\operatorname{sign}\operatorname{Im} s$ to be 0 in the latter region. To find z_∞, we must again require that the t^0 term in the large-t expansion be equal to the phase at the stationary point, $\phi_s = \arg F(z_0)$. In the generic case, when $N_- \neq 0$, we can do this simultaneously for the $t \to \pm\infty$ limits, thereby obtaining a pair of equations and solving for the real and imaginary parts independently,

$$\begin{aligned}
\operatorname{Re} z_\infty &= +\frac{1}{2N_-}(S_+ - 2A_+ - 2D_-^{(\psi)} - 2S^{(\psi)}) \bmod 4\\
&\quad -\frac{1}{2\pi N_-}[(A_+ + A_- - S_+/2 - S_-/2 - D_+^{(\psi)} - D_-^{(\psi)})(\theta_{+\infty} + \theta_{-\infty} - \pi) \bmod 2\pi],\\
\operatorname{Im} z_\infty &= \frac{\phi_s}{\ln|s_0/s|} - \frac{\pi \operatorname{sign}\operatorname{Im} s}{2N_- \ln|s_0/s|}(S_+ - 2A_+ - 2D_-^{(\psi)} - 2S^{(\psi)}) \bmod 4\\
&\quad +\frac{1}{2\ln|s_0/s|}[(A_+ + A_- - S_+/2 - S_-/2 - D_+^{(\psi)} - D_-^{(\psi)})(\theta_{-\infty} - \theta_{+\infty}) \bmod 2\pi]\\
&\quad +\frac{\operatorname{sign}\operatorname{Im} s}{2N_- \ln|s_0/s|}[(A_+ + A_- - S_+/2 - S_-/2 - D_+^{(\psi)} - D_-^{(\psi)})(\theta_{+\infty} + \theta_{-\infty} - \pi) \bmod 2\pi].
\end{aligned} \tag{6.18}$$

In deriving these formulas, we have again implicitly used the condition that $\theta_{\pm\infty} \in [-\frac{\pi}{2}, \frac{\pi}{2}]$. As in the Euclidean case, these values may be shifted in order to match the appropriate asymptote,

$$\delta z_\infty = \frac{n_1 - n_2}{N_-} + i\frac{\pi(n_1 + n_2)}{\ln|s_0/s|} + i\frac{\pi(n_2 - n_1)\operatorname{sign}\operatorname{Im} s}{N_- \ln|s_0/s|}, \tag{6.19}$$

where $n_{1,2}$ are integers.

We postpone a discussion of the $N_- = 0$ case to Sec. VI C.

The differing asymptotic forms require us to generalize the [3/2] Padé form (3.16) to

$$z_p(t) = z_s + ie^{i\theta_s}t + \frac{e^{i\theta_s}t^2(\hat{a}_2 + i\hat{b}_2\hat{a}_3 t)}{1 + i\hat{b}_1 t + \hat{b}_2 t^2}. \tag{6.20}$$

Matching to a quadratic contour at small t requires three coefficients, and to a linear asymptotic contour at large t an additional two coefficients (more precisely, one complex coefficient and one phase). A [2/1] Padé approximation does not have enough free coefficients to match both limits, so a [3/2] Padé approximation is the simplest possible one. (A similar result is true in the Euclidean region, though the argument is more subtle.) However, a [3/2] Padé form has one additional parameter, that we can use to fix the cubic terms in the contour as well, so as to make the $\mathcal{O}(t^5)$ (and in principle the $\mathcal{O}(t^6)$) terms in the expansion of the integrand have the phase of the stationary point as well. As we are not truncating the contour at cubic order, however, the equation for $y''(0)$ also involves $x^{(3)}(0)$, and additional equations also involve higher derivatives. In order to simplify the structure of the equations, it is convenient to perform a nonlinear transformation to a new set of parameters $\{\alpha_i, \beta_i\}$ via

$$\begin{aligned}
a_s &= \alpha_3 e^{-i\theta_s} - 1,\\
d_M &= \alpha_2(z_s - \beta_1) + e^{i\theta_s}a_s^2,\\
\hat{a}_2 &= \alpha_2,\\
\hat{a}_3 &= a_s,\\
\hat{b}_1 &= i d_M^{-1}(\beta_2(z_s - \beta_1) + i\alpha_2 e^{i\theta_s}a_s),\\
\hat{b}_2 &= -d_M^{-1}e^{i\theta_s}(\alpha_2^2 + i\beta_2 a_s),
\end{aligned} \tag{6.21}$$

In these equations, θ_s is given by Eq. (6.6); matching the asymptotic behavior and taking $\theta_{\pm\infty}$ from Eq. (6.17), we can fix α_3 up to an overall magnitude,

$$\alpha_3 = \rho_3(e^{i\theta_{+\infty}}\Theta(t) + e^{i\theta_{-\infty}}\Theta(-t)), \tag{6.22}$$

as well as β_1,

$$\beta_1 = z_\infty. \tag{6.23}$$

The improvements from adjusting ρ_3 are marginal, and trying to solve for it requires solving much higher-order polynomial equations, so we again simply fix it to 1. Requiring the integrand to be of stationary phase through cubic order fixes the real part of α_2,

$$\mathrm{Re}\,\alpha_2 = \frac{\mathrm{Re}\,D_3}{6D_2} = \mathrm{Re}\,c_2. \tag{6.24}$$

(Recall that D_2 is real by construction.) Requiring the integrand to be of stationary phase through quartic order fixes the imaginary part of α_2 in terms of derivatives of the integrand along with β_2,

$$\mathrm{Im}\,\alpha_2 = \frac{\mathrm{Im}\,D_4}{8\mathrm{Re}\,D_3} - \frac{\mathrm{Im}\,D_3}{4D_2} + \frac{3D_2}{\mathrm{Re}\,D_3}\mathrm{Re}\,\beta_2. \tag{6.25}$$

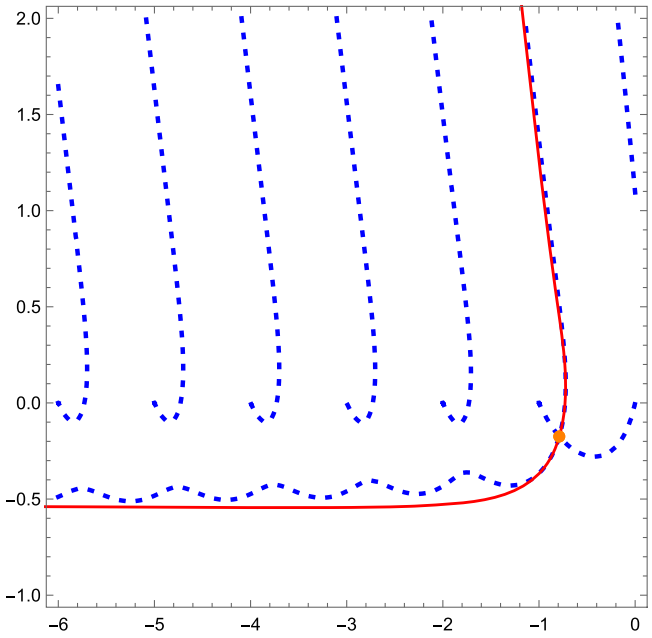

FIG. 22. The [3/2] Padé approximation to the contour of stationary phase $e^{i\phi_s}$ (solid red) for the integrand $F_1(z,s)$ of Eq. (2.2) with $s = 1 + i\delta$. The exact contours of this phase are also shown (dotted blue). The saddle point is indicated by a large orange dot.

Requiring stationarity through $\mathcal{O}(t^6)$ would give an additional pair of equations for the real and imaginary parts of β_2. However, these equations are of rather high order, and do not always admit solutions. Furthermore, the solutions to these equations may yield contours with loops. The best approach to fixing β_2 appears to be minimizing a weighted sum of the square of the following deviation from stationarity at quintic order,

$$\begin{aligned}
&-\frac{3D_2^2}{2\mathrm{Re}\,D_3}(\mathrm{Re}\,\beta_2)^2 + \left(\frac{D_2\mathrm{Im}\,D_4}{4\mathrm{Re}\,D_3} - \frac{1}{2}\mathrm{Im}\,D_3\right)\mathrm{Re}\,\beta_2 \\
&-\frac{1}{3}\mathrm{Re}\,D_3\mathrm{Im}\,\beta_2 - \frac{\mathrm{Im}\,D_3\mathrm{Im}\,D_4}{32D_2} + \frac{5(\mathrm{Im}\,D_4)^2}{384\mathrm{Re}\,D_3} \\
&+\frac{(\mathrm{Im}\,D_3)^2\mathrm{Re}\,D_3}{96D_2^2} + \frac{(\mathrm{Re}\,D_3)^3}{72D_2^2} - \frac{\mathrm{Re}\,D_3\mathrm{Re}\,D_4}{36D_2} + \frac{1}{120}\mathrm{Re}\,D_5 \\
&+D_2\mathrm{Re}\left[\frac{\alpha_2^3 + 2i\alpha_2\beta_2 a_s + \beta_2^2 e^{-i\theta_s}(z_s - z_\infty)}{a_s^2 + \alpha_2 e^{-i\theta_s}(z_s - z_\infty)}\right],
\end{aligned} \tag{6.26}$$

the square of the relative phases of the denominator terms,

$$\arg(-i\hat{b}_2/\hat{b}_1), \tag{6.27}$$

and the square of the relative phases of the numerator terms,

$$\arg(-i\hat{a}_2/(\hat{b}_2\hat{a}_3)). \tag{6.28}$$

The minimization is over the real and imaginary parts of β_2, after substituting in Eqs. (6.22), (6.24), and (6.25). A good heuristic weights the quintic significantly more than the denominator's relative phase, which in turn is weighted more than the numerator's relative phase. Because α_3, which depends on the sign of t, appears implicitly on the right-hand side of Eq. (6.26) as well explicitly in the relative phases, all parameters will likewise acquire a dependence on that sign.

The resulting [3/2] Padé contour for $s = 1 + i\delta$ is shown in Fig. 22. For negative imaginary parts of $z(t)$, the contour

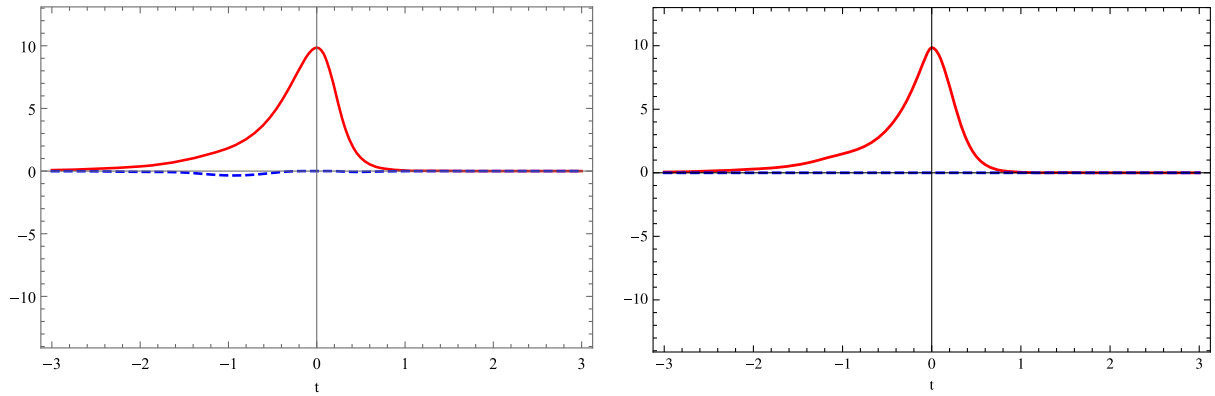

FIG. 23. The real (red) and imaginary (dashed blue) parts of the integrand $F_1(z,s)$ of Eq. (2.2) for $s = 1 + i\delta$, after dividing out the phase at the saddle point, along (a) the [3/2] Padé approximation to the contour of stationary phase passing through the saddle point (b) the exact contour of stationary phase.

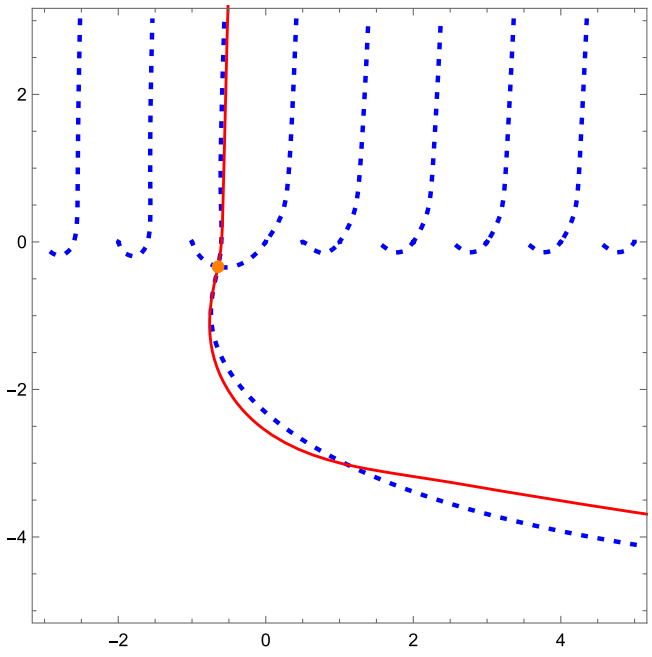

FIG. 24. The [3/2] Padé approximation to the contour of stationary phase $e^{i\phi_s}$ (solid red) for the integrand $F_1(z,s)$ of Eq. (2.2) with $s = 5 + i\delta$. The exact contours of this phase are also shown (dotted blue). The saddle point is indicated by a large orange dot.

is asymptotically parallel to the real axis. Accordingly, it properly includes contributions from all poles, and repairs the defect in the quadratic contour. On a linear scale, the values of the real and imaginary parts of the integrand along the Padé contour are quite similar to those along the quadratic contour, because the values are very small in regions where the contours differ. In Fig. 23(a), we show the real and imaginary parts of the integrand along the Padé contour, after dividing out by the phase $e^{i\phi_s}$ at the saddle point. Figure 23(b) shows the same parts along the exact contour of stationary phase; the parametrization of the exact contour is different (for $t > 0$, the imaginary part of the contour is chosen to be t, while for $t < 0$, the real part is chosen to be t), leading to a somewhat different shape, but the absence of oscillations in the real part, and the small value of the imaginary part in both parts of the figure show that the Padé contour is a very good approximation to the exact one.

B. Above threshold

The approach described in the previous subsection also works above threshold. The integral has a branch cut starting at threshold, so here we need to give an infinitesimal imaginary part to the parameter s in order to obtain the integral's value as well as for finding contours. We will again take this imaginary part to be positive; taking it negative would complex-conjugate the result and all the contours we find as well. The Padé approximation contour for $s = 5 + i\delta$ is shown in Fig. 24, and the integrand along it (with the phase at the saddle point divided out) is shown in Fig. 25(a). As we can see, although the contour deviates noticeably from the exact contour in between small and very large negative values of t, the integrand does not oscillate significantly, and hence this deviation will have little effect on the convergence of the integration. We show the integrand along the exact contour in Fig. 25(b), with the imaginary part of the contour again taken to be t.

C. Parallel asymptotes

As we saw in Sec. V D, the case $N_- = 0$ requires special treatment, because the asymptotes are parallel, and so one must require the intercept for the asymptotic form to have an imaginary part. Otherwise, the Padé contours are unexceptional in the Euclidean region: they properly enclose all the poles enclosed by the "textbook" contour selected by MB. The behavior of the integrand along these contours is likewise unexceptional. In the Minkowski region, the situation is different. As we can see from Eqs. (6.16) and

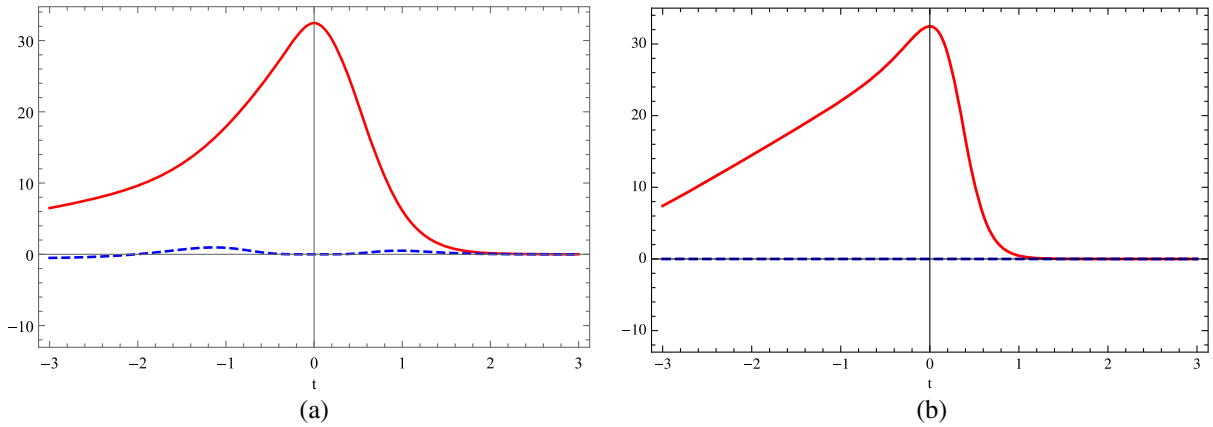

FIG. 25. The real (red) and imaginary (dashed blue) parts of the integrand $F_1(z,s)$ of Eq. (2.2) for $s = 5 + i\delta$, with the phase at the saddle point divided out, along (a) the Padé approximation to the contour of stationary phase passing through the saddle point (b) the exact contour of stationary phase.

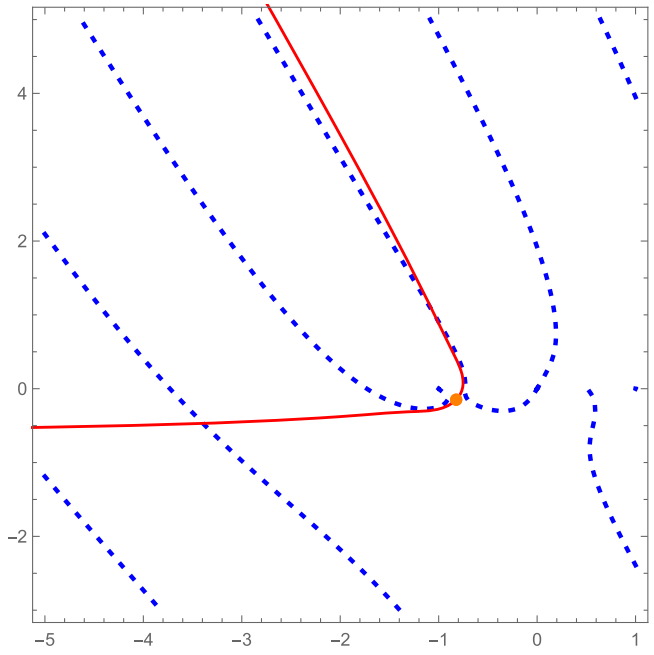

FIG. 26. The [3/2] Padé approximation to the contour of stationary phase $e^{i\phi_s}$ (solid red) for the integrand $F_5(z,s)$ of Eq. (5.7) with $s = 1 + i\delta$. The exact contours of this phase are also shown (dotted blue). The saddle point is indicated by a large orange dot.

(6.17), the asymptotes for $t \to \pm\infty$ are parallel to each other, but not to the real axis. This means that a single contour cannot enclose all poles (in general, each contour will enclose only a single pole). An example, the integrand of Eq. (5.7) with $s = 1 + i\delta$, is shown in Fig. 26.

As in the case of closed contours considered in Sec. V E, from a practical point of view it doesn't make sense to use the ensemble of exact contours. (One would again be better off computing the residues analytically and summing over them.) The approximate Padé contour can instead be chosen to have one of the asymptotes parallel to the real axis, thereby enclosing all poles, at the price of small oscillations in the tail of the integrand along the contour. This can be done by choosing $\theta_{-\infty}$ to be $\pi/2$ (for $\operatorname{sign} \operatorname{Im} s > 0$), and then using a modified expression for z_∞,

$$\begin{aligned}\operatorname{Re} z_\infty = {} & \frac{\phi_s}{\pi} - \frac{\ln|s_0/s| \operatorname{Im} z_\infty}{\pi} \\ & + \frac{1}{2}(S_+ - 2A_+ - 2D_-^{(\psi)} - 2S^{(\psi)}) \bmod 4 \\ & - \frac{1}{2\pi}[(A_+ + A_- - S_+/2 - S_-/2 - D_+^{(\psi)} - D_-^{(\psi)}) \\ & \times (2\theta_{+\infty} - \pi) \bmod 2\pi], \end{aligned} \tag{6.29}$$

where $\operatorname{Im} z_\infty$ can be chosen with some freedom; a good heuristic is again to take it to be of order $1/\operatorname{Re} c_2$.

VII. INTEGRANDS WITHOUT EXTREMA

As mentioned in Sec. V, an integrand may have *no* real interval in which the integrand has an extremum. In this case, however, there is always a zero of the integrand in any given interval between poles. Let us consider the simplest (and most generic) case of this type, where the integrand has a simple zero independent of the value of the parameter s. An example of such an integral is

$$I_7(s) = \frac{1}{2\pi i}\int_{c_0-i\infty}^{c_0+i\infty} dz F_7(z,s), \tag{7.1}$$

where

$$F_7(z,s) = (-s)^{-z}\frac{\Gamma^3(-z)\Gamma(3+z)\psi^{(2)}(z)}{\Gamma(-2z)}, \tag{7.2}$$

which is just $F_1(z,s)$ of Eq. (2.2), multiplied by additional polygamma and polynomial factors.

Consider first the Euclidean region; the integrand is real for real z, but has no finite extrema as displayed in Fig. 27. Instead, the integrand has complex stationary points; they come in complex-conjugate pairs. Moreover, while there are still contours of stationary phase, the integrand is no longer necessarily real on them. The integral is nonetheless real.

How is this possible? In the generic case discussed in previous sections, a contour of stationary phase comes in from infinity, passing through a stationary point, and heads back out to infinity. When the function has a zero, however, contours of stationary phase can end there. In the case at hand, the full contour of integration will actually consist of two separate contours of integration, complex conjugates joined at the zero of the integrand. The phase is stationary on each separate contour, but different; indeed, the phase of the integrand on the contour in the lower-half plane is the

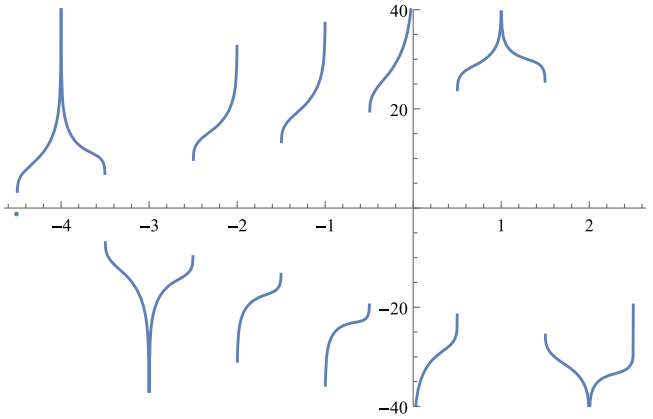

FIG. 27. The behavior of the integrand $F_7(z,s)$ of Eq. (7.2), along the real axis. The plot displays sln_{20}(integrand), with $s = -\frac{1}{20}$.

complex conjugate of the phase on the contour in the upper-half plane.

One could choose to deform the textbook contour to one passing through the two stationary points using a quadratic approximation, without worrying where exactly it crosses the real axis. However, this will still leave substantial oscillations in the integrand near the real axis. To do better, we seek a contour that passes through the stationary points and also through the zero of the integrand on the real axis. We join two half-contours in each half-plane, taking the half-contour in the lower half-plane to be the complex conjugate of that in the upper half-plane. Each half-contour will end at the zero. To best approximate the (half-)contour of stationary phase, we match the tangent at the stationary point, and also the initial direction at the integrand's zero. This requires six real parameters: the real and imaginary parts of the zero location and the stationary point, and the two angles giving the directions at those points. This is exactly the number of parameters available in a quadratic curve,

$$z_h(t) = z_0 + e^{i\theta_0}(i a_1 t + a_2 t^2), \tag{7.3}$$

where a_1 is real but a_2 is complex. In this case, we do not have enough parameters to match the curvature at the stationary point, unlike contours considered in previous sections. We give below the formulas for a half-contour in the upper half-plane; a similar set with appropriate replacements ($\theta_{+\infty} \to \theta_{-\infty}$, etc.) gives the half-contour in the lower half-plane.

To derive formulas for the parameters in Eq. (7.3), expand the imaginary part of the integrand after dividing out the phase at the stationary point, obtaining

$$a_1 \mathrm{Im}\left[\frac{(iF'(z_0))}{F(z_s)} e^{i\theta_0}\right] t + \mathcal{O}(t^2). \tag{7.4}$$

Let us restrict attention here to integrands with simple zeros, so that $F'(z_0)$ does not vanish. (The generalization to higher-order zeros is reasonably straightforward.) Requiring the coefficient of t to vanish determines the initial direction θ_0 along the half-contour,

$$\theta_0 = \arg(-iF(z_s)/F'(z_0)). \tag{7.5}$$

The tangent angle θ_s at the stationary point is given by Eq. (6.6) (up to a possible rotation by $\pi/2$); we can solve for a_1 and a_2 in terms of the two angles and the locations of the zero and the stationary point,

$$\begin{aligned} a_1 &= \frac{2\mathrm{Re}[e^{-i\theta_s}(z_s - z_0)]}{\sin(\theta_s - \theta_0)}, \\ a_2 &= e^{-i\theta_0}(z_s - z_0) - i a_1. \end{aligned} \tag{7.6}$$

To match the asymptotic behavior as well, and thereby make the contour more robust, we again turn to a [3/2] Padé approximation, which it is here convenient to write in the form

$$\begin{aligned} z_h(t) = z_0 + (z_s - z_0)t + t(t-1) \\ \times \frac{\mathring{a}_2 + \mathring{b}_2 \mathring{a}_3 (t-1)}{1 + \mathring{b}_1 (t-1) + \mathring{b}_2 t (t-1)}. \end{aligned} \tag{7.7}$$

In this form, the parameter t has been rescaled to put the saddle point at $t = 1$. As in Sec. VI, it is convenient to make a nonlinear transformation to a new set of (real) parameters $\{\rho_{2,3,b}\}$,

$$\begin{aligned} \mathring{a}_2 &= i\rho_2 e^{i\theta_s} - (z_s - z_0), \\ \mathring{a}_3 &= i\rho_3 e^{i\theta_{+\infty}} - (z_s - z_0), \\ d_Z &= \mathring{a}_3^2 - (i\rho_3 e^{i\theta_{+\infty}} + \mathring{z}_\infty - z_s)(i\rho_b e^{i\theta_0} - (z_s - z_0)), \\ \mathring{b}_1 &= 1 - d_Z^{-1}(\mathring{a}_3^2 + (\mathring{z}_\infty - z_0)\mathring{a}_2), \\ \mathring{b}_2 &= d_Z^{-1}(i\rho_3 e^{i\theta_{+\infty}}(\mathring{a}_2 + i\rho_b e^{i\theta_0} - (z_s - z_0)) \\ &\quad + (z_s - z_0)^2 + \rho_2 \rho_b e^{i(\theta_s + \theta_0)}). \end{aligned} \tag{7.8}$$

In these equations, θ_s is given by Eq. (6.6); θ_0 by Eq. (7.5); $\theta_{+\infty}$ by Eq. (6.17); and z_∞ by

$$\begin{aligned} z_\infty = \frac{\phi_s \,\mathrm{sign}\,\mathrm{Im}\, z_s}{\pi N_-} + \frac{(S_+ - 2A_+ - 2D_-^{(\psi)} - 2S^{(\psi)}) \bmod 4}{2(N_- + \mathrm{sign}\,\mathrm{Im}\, s)} \\ - \frac{1}{(N_- + \mathrm{sign}\,\mathrm{Im}\, s)\pi}\left[(A_+ + A_- - S_+/2 - S_-/2 - D_+^{(\psi)} \right. \\ \left. - D_-^{(\psi)})\left(\theta_\infty - \frac{\pi}{2}\right) \bmod 2\pi\right], \quad N_- \neq -\mathrm{sign}\,\mathrm{Im}\, s. \end{aligned} \tag{7.9}$$

As in the generic situation, this value may be shifted in order to match onto the desired asymptotic contour, by multiples of $2/(N_- + \mathrm{sign}\,\mathrm{Im}\, s)$. (In the case when $N_- = -\mathrm{sign}\,\mathrm{Im}\, s$, z_∞ must be chosen imaginary, and we can use the last equation in Eq. (4.15), along with possible shifts given in the text below that equation.) The forms in Eq. (7.8) then give a contour that automatically satisfies the correct asymptotic form; that has the correct initial direction at z_0; and that has the correct tangent at z_s.

As in the generic case, we fix ρ_3 to 1. We can fix ρ_2 and ρ_b by minimizing the square of the following deviation from stationarity of the cubic term in the expansion of the integrand around the stationary point,

$$\begin{aligned} + \mathrm{Re}\left[\frac{(\rho_2 e^{i\theta_s} - \rho_3 e^{i\theta_{+\infty}})^2}{i\rho_3 e^{i\theta_{+\infty}} + \mathring{z}_\infty - z_s}\right] + \mathrm{Re}\left[d_Z^{-1} \frac{(\mathring{a}_3^2 + \mathring{a}_2(\mathring{z}_\infty - z_0))^2}{i\rho_3 e^{i\theta_{+\infty}} + \mathring{z}_\infty - z_s}\right] \\ - \frac{\mathrm{Re}\, D_3}{6 D_2}, \end{aligned} \tag{7.10}$$

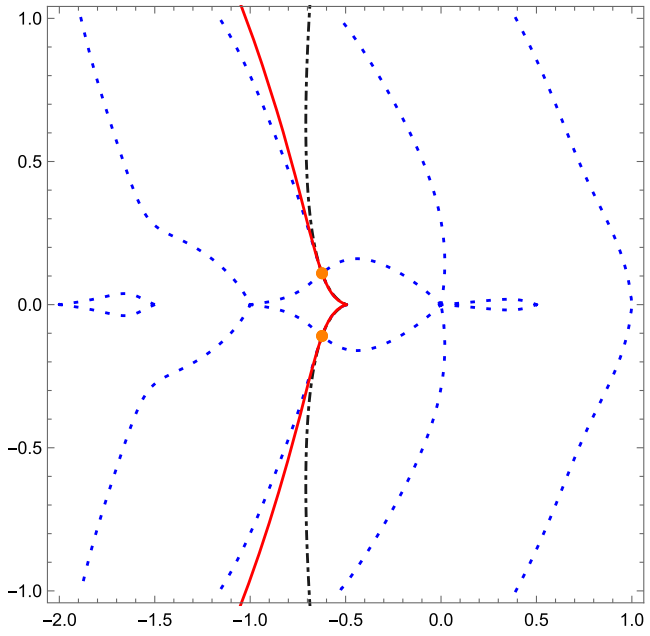

FIG. 28. The joined quadratic (dot-dashed dark gray) and joined [3/2] Padé approximations (solid red) to the contour of stationary phase for the integrand $F_7(z,s)$ of Eq. (7.2) with $s=-\frac{1}{20}$. The exact contours of constant phase are also shown (dotted blue). The saddle points are indicated by large orange dots.

along with the square of the relative phases of the denominator terms,

$$\arg(\mathring{b}_2/\mathring{b}_1), \tag{7.11}$$

and the square of the relative phases of the numerator terms,

$$\arg(\mathring{a}_2/(\mathring{b}_2\mathring{a}_3)). \tag{7.12}$$

The minimization is after substituting the expressions in Eq. (7.8). For certain integrands or values of the parameter s, this approach appears to avoid looping contours that would otherwise arise. A good heuristic weights the cubic (7.10) significantly more than the denominator's relative phase, which in turn is weighted more than the numerator's relative phase. As with the reparametrizations and the fixing of θs, the minimization should be carried out independently for the upper- and lower-half planes.

The joined quadratic and joined [3/2] Padé contours for $F_7(z,s=-\frac{1}{20})$ are shown in Fig. 28, while the integrand along the joint Padé contour is shown in Fig. 29, and contrasted with the behavior along the "textbook" MB contour $\mathrm{Re}\,z=-\frac{1}{2}$. The phase at the upper saddle point is divided out for $t>0$, and that at the lower saddle point for $t<0$.

The exact contours are shown in Fig. 30. The contours passing through the saddle points at $-0.623407\pm 0.109501i$ illustrate another potential complication with exact contours: in addition to ending at zeros on the real axis, they can end at zeros off in the complex plane without ever making it out to infinity. Their use would then necessitate finding the zeros and gluing on additional contours starting there. In contrast, the Padé contour smoothly interpolates to a curve reaching infinity, at the price of very small oscillations in the tail of the integrand. These oscillations do not disturb our ability to use the contour to calculate the integral precisely and efficiently.

The same approach works in the Minkowski region as well; here of course, the two half-contours will no longer be complex conjugates. The [3/2] Padé contours for $s=1+i\delta$ and $s=5+i\delta$ are shown in Fig. 31, while the behavior of the integrands along these contours are shown in Fig. 32. They are contrasted with the behavior along the "textbook" MB contour $\mathrm{Re}\,z=-\frac{1}{2}$. The integrand along the

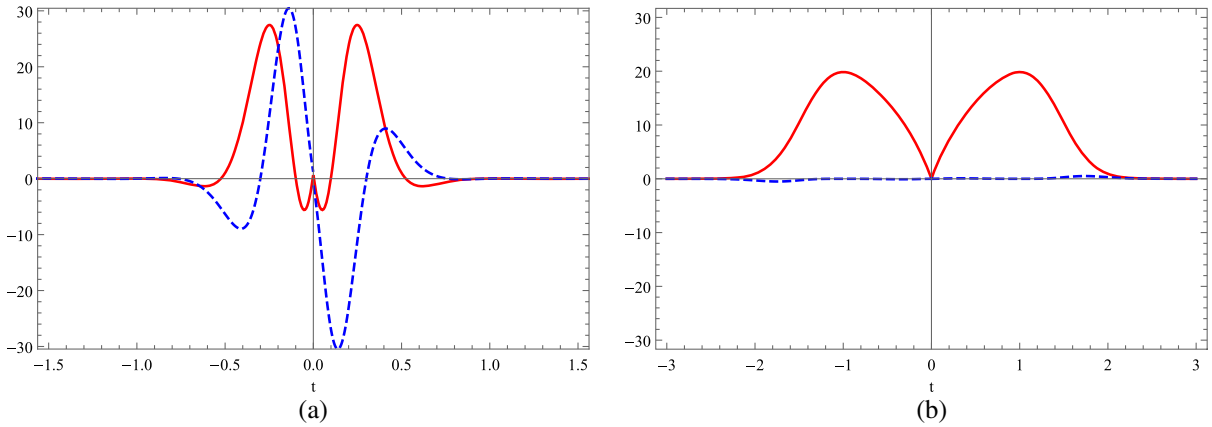

FIG. 29. The real (red) and imaginary (dashed blue) parts of the integrand $F_7(z,s)$ of Eq. (7.2) for $s=-\frac{1}{20}$ (a) along the simple contour $\mathrm{Re}\,z=-\frac{1}{2}$ (b) along the joined Padé approximations, to the contour of stationary phase, with the phases at the saddle points divided out.

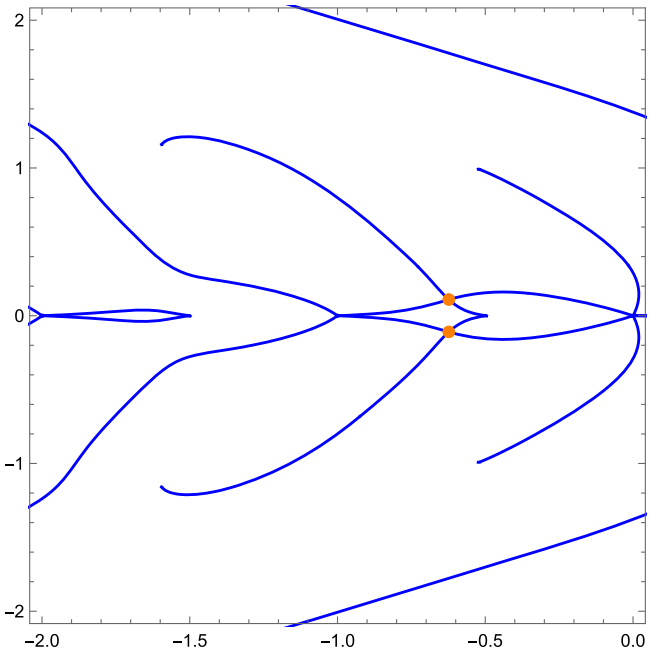

FIG. 30. Exact contours (solid blue) of stationary phase for the integrand $F_7(z,s)$ of Eq. (7.2) with $s=-\frac{1}{20}$. The saddle points are indicated by large orange dots.

latter contour is again not absolutely convergent, and hence not numerically stable. A different contour is again required for a convergent numerical integration, and the Padé contour provides an efficient one. (Note that I_7 has an imaginary part already starting at $s=0$, and not just at $s=4$.)

VIII. EVALUATING INTEGRALS

In the previous sections, we have described simple approximations to the exact contours of stationary phase in both the Euclidean and Minkowski regions. We turn now to a brief discussion of how to evaluate the integrals along these contours, postponing a more complete investigation to future work.

The simplest approach to evaluating the integral using any of the contours is with an adaptive numerical routine, such as `gsl_integration_qagiu` and `gsl_integration_qagil` from the GNU Scientific Library (GSL) [51].

Another approach to evaluating the integral along the [3/2] Padé contour takes advantage of the exponential decay in the integrand from the saddle point out to $t\to\pm\infty$, and uses Gaussian quadrature with a finite number of evaluation points based on orthogonal polynomials for an appropriate weight function. At small t, the integrand behaves like e^{-ct^2}, while at large t, it behaves like $e^{-c't}$, so the classical weight functions are not optimal for us. Instead, motivated by the observation that

$$\Gamma(-z)\Gamma(1+z)=-\frac{\pi}{\sin\pi z}, \tag{8.1}$$

so that

$$\Gamma\left(\frac{1}{2}-iy\right)\Gamma\left(\frac{1}{2}+iy\right)=\pi\,\mathrm{sech}\,\pi y, \tag{8.2}$$

we take $\mathrm{sech}u$ as our weight function. It has the required behavior at small and large u.

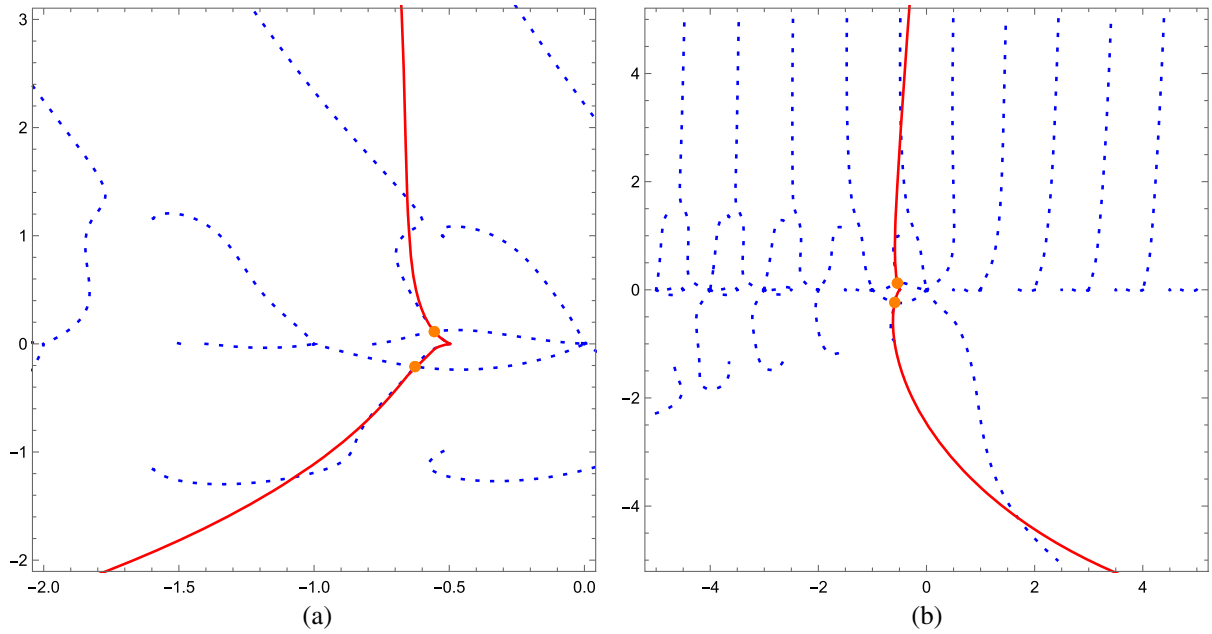

FIG. 31. The joined [3/2] Padé approximations (solid red) to the contour of stationary phase for the integrand $F_7(z,s)$ of Eq. (7.2) with (a) $s=1+i\delta$ (b) $s=5+i\delta$. The exact contours of constant phase are also shown (dotted blue). The saddle points are indicated by large orange dots.

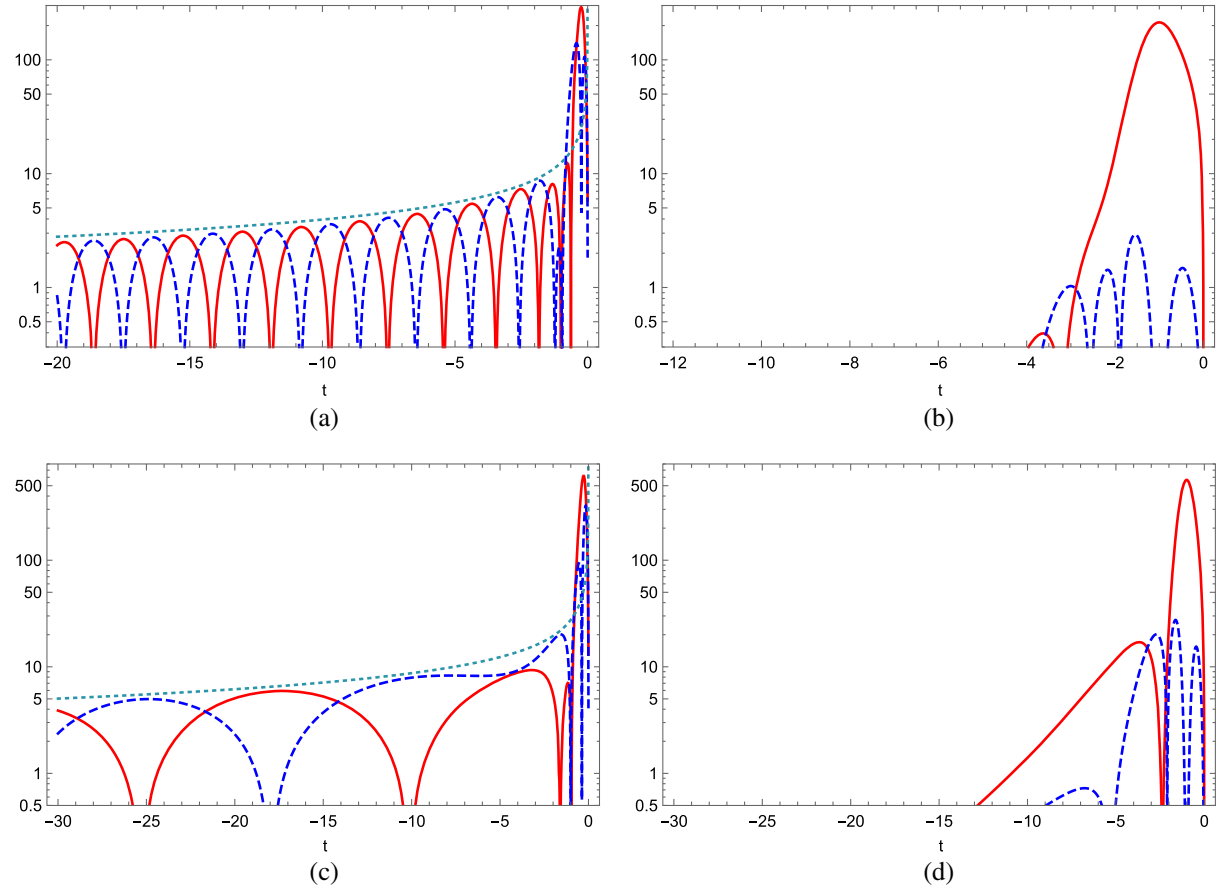

FIG. 32. The absolute values of the real (red) and imaginary (dashed blue) parts of the integrand of Eq. (7.2), shown on a log scale, for (a) $s = 1 + i\delta$ along the simple contour $\mathrm{Re}\, z = -\frac{1}{2}$ (b) $s = 1 + i\delta$ along the joined Padé approximations to the contour of stationary phase (c) $s = 5 + i\delta$ along the simple contour $\mathrm{Re}\, z = -\frac{1}{2}$ (d) $s = 5 + i\delta$ along the joined Padé approximations to the contour of stationary phase. The phases at the saddle points are divided out before taking real and imaginary parts. In (a) and (c), the dotted (dark turquoise) curve shows a curve decreasing as $t^{-1/2}$.

Because the coefficients c and c' governing small-t and large-t behavior are not the same, in principle we ought to interpolate between different linear arguments for small and large t. We could do this, for example, via

$$f_i(t) = f_\infty t + \left(\sqrt{2f_2} - f_\infty\right)\frac{t}{1 + b_3 t}, \tag{8.3}$$

where f_∞ and f_2 will be extracted from our integrand below, and b_3 is an additional parameter. (There is no

TABLE I. Number of evaluations required to obtain a relative error of 10^{-8} for a variety of integrals, using several integration methods. A missing entry indicates that the integral is not convergent numerically using the given method.

		Integration contour and method			
		MB	Tangent	Padé	Padé
Integral	Value	GSL	GSL	GSL	Gauss-Legendre
$I_1(-\frac{1}{20})$	0.04958745585	195	195	75	16
$I_1(-20)$	5.639661654	135	135	105	19
$I_1(1 + i\delta)$	−1.2091995762	—	930	1080	80
$I_1(5 + i\delta)$	4.30408941−14.04962946i	—	—	660	160
$I_7(-\frac{1}{20})$	−1.954168464	225	165	195	26
$I_7(-20)$	−35.72650854	135	165	165	19
$I_7(1 + i\delta)$	2.831441537 + 17.99925456i	—	1140	780	159
$I_7(5 + i\delta)$	−27.40504335 + 37.26381174i	—	—	720	200

need to have an analytic form for the inverse function, so other forms could be used.)

The required coefficients f_∞ and f_2 describe the large- and small-t behavior of the integrand $F(z(t))$, respectively,

$$f_2 = -\frac{F''(z_s)}{2F(z_s)},$$
$$f_\infty = \left| \ln\left|\frac{s_0}{-s}\right| \sin\theta_\infty + (N_- + \operatorname{sign}\operatorname{Im} s)\pi\cos\theta_\infty \right|. \quad (8.4)$$

(Recall that with our conventions, $z(0)$ is the saddle point z_s.) However, it turns out (surprisingly) that the integration is ultimately *much* more efficient if we do not interpolate, but rather take

$$\operatorname{sech} f_\infty t/4, \quad (8.5)$$

as our weight function.

We can next perform two changes of variables: first, the change of variables $u = \operatorname{atanh} v$ takes us from integrating over $[0, \infty)$ to integrating over the interval [0, 1]. The new weight function (including the Jacobian) is $(1-v^2)^{-1/2}$, which would suggest the use of Gauss-Chebyshev quadrature, were it not for the region of integration failing to match the required $[-1, 1]$. Instead, we can make another change of variables, $v = \cos\omega$, to arrive at the integral,

$$I_n = \frac{4}{f_\infty}\int_0^{\pi/2} d\omega F((4\operatorname{atanh}\cos\omega)/f_\infty) \times z_p'(4(\operatorname{atanh}\cos\omega)/f_\infty), \quad (8.6)$$

in the upper half-plane (and a similar integral with $\cos\omega$ replaced by $-\cos\omega$ for the lower half-plane) for the original Mellin-Barnes integrand $F(z)$. The integral I_n can be computed efficiently via Gauss-Legendre quadrature, with an n-point evaluation at the roots of the nth Legendre polynomial $P_n(x)$, and the weight for the jth root [52] given by

$$\frac{2}{(1-x_j^2)[P_n'(x_j)]^2}. \quad (8.7)$$

Other techniques, such as recursive subdivision, may also be appropriate, but we have not explored them.

Table I gives examples of evaluating the Mellin-Barnes integrals I_1 (2.1) and I_7 (7.1) using both the contour chosen by MB, as well as the tangent and Padé contours, all using the GSL routines mentioned earlier, as well as an evaluation using the Padé contour and the Gauss-Legendre approach. In the Euclidean region, the Padé contour provides a more efficient evaluation, especially within the Gauss-Legendre approach. In the Minkowski region, it is again more efficient where other contours can be used, and provides a reliable means of evaluating the integrals even when linear contours fail to provide a numerically convergent result.

IX. CONCLUSIONS

In this paper, we have reexamined the numerical evaluation of Mellin-Barnes integrals. Contours chosen by the MB or MBresolve packages are not always suitable for numerical evaluation. Using contours of stationary phase, or approximations thereto, resolves problems that arise in numerical evaluation. We discussed the computation of exact contours of stationary descent for one-dimensional integrals, as well as several approximations which are likely of greater practical importance. The [3/2] Padé approximations (3.16), (6.20), and (7.7) to contours of stationary phase are likely to be the most robust and widely useful of these approximations. A remapping and Gauss-Legendre quadrature appears to be an efficient means of evaluating integrals using the Padé contour.

We hope to extend these ideas to the more practically important multidimensional case in future work. Beyond one complex dimension, the contours of steepest descent are replaced by 'surfaces of steepest descent'. The stationarity of phase itself is not sufficient to fix these surfaces, which will require generalizing the derivations in this paper. Furthermore, the integrands of interest are in general not separable into functions of the different complex variables, and so will have singularities away from the real axes. The Padé approximations can be generalized, but they may not automatically avoid these new singularities, and must be constrained to do so. The extent to which one can or must match to asymptotic forms also remains to be determined. We believe that these issues can be addressed, but further development beyond that outlined in this paper is required.

ACKNOWLEDGMENTS

We thank Valery Yundin for collaboration in early stages of this research. J. G. and T. J. also thank Tord Riemann, Ievgen Dubovyk, and Johann Usovitsch for discussions. J. G.'s research is supported by the Polish National Science Center under Grant Agreement No. DEC–2013/11/B/ST2/04023. D. A. K. thanks the Ambrose Monell Foundation for its support of his stay at the Institute for Advanced Study.

[1] V. A. Smirnov, Springer Tracts Mod. Phys. **211**, 1 (2004).
[2] A. Freitas, Prog. Part. Nucl. Phys. **90**, 201 (2016).
[3] V. A. Smirnov, Phys. Lett. B **460**, 397 (1999); V. A. Smirnov and O. L. Veretin, Nucl. Phys. **B566**, 469 (2000).
[4] J. B. Tausk, Phys. Lett. B **469**, 225 (1999).
[5] M. Czakon, Comput. Phys. Commun. **175**, 559 (2006).
[6] A. Smirnov and V. Smirnov, Eur. Phys. J. C **62**, 445 (2009).
[7] MBtools webpage, https://mbtools.hepforge.org/.
[8] J. Gluza, K. Kajda, and T. Riemann, Comput. Phys. Commun. **177**, 879 (2007); J. Gluza, K. Kajda, T. Riemann, and V. Yundin, Eur. Phys. J. C **71**, 1516 (2011).
[9] I. Dubovyk, J. Gluza, T. Riemann, and J. Usovitsch, arXiv:1607.07538.
[10] M. Czakon, `MBasymptotics.m` at https://mbtools.hepforge.org/.
[11] D. Kosower, `barnesroutines.m` at https://mbtools.hepforge.org/.
[12] E. E. Boos and A. I. Davydychev, Teor. Mat. Fiz. **89**, 56 (1991) [Theor. Math. Phys. **89**, 1052 (1991)].
[13] A. I. Davydychev, J. Phys. A **25**, 5587 (1992).
[14] N. I. Usyukina and A. I. Davydychev, Phys. Lett. B **305**, 136 (1993).
[15] S. Actis, M. Czakon, J. Gluza, and T. Riemann, Phys. Rev. D **78**, 085019 (2008); Phys. Rev. Lett. **100**, 131602 (2008); M. Czakon, J. Gluza, and T. Riemann, Nucl. Phys. **B751**, 1 (2006).
[16] G. Heinrich, T. Huber, D. A. Kosower, and V. A. Smirnov, Phys. Lett. B **678**, 359 (2009); R. N. Lee, A. V. Smirnov, and V. A. Smirnov, J. High Energy Phys. 04 (2010) 020; P. A. Baikov, K. G. Chetyrkin, A. V. Smirnov, V. A. Smirnov, and M. Steinhauser, Phys. Rev. Lett. **102**, 212002 (2009).
[17] A. V. Smirnov, V. A. Smirnov, and M. Steinhauser, Phys. Rev. Lett. **104**, 112002 (2010).
[18] J. Gluza, A. Mitov, S. Moch, and T. Riemann, J. High Energy Phys. 07 (2009) 001.
[19] M. Beneke, T. Huber, and X.-Q. Li, Nucl. Phys. **B811**, 77 (2009); G. Bell and T. Huber, J. High Energy Phys. 12 (2014) 129.
[20] P. Bärnreuther, M. Czakon, and P. Fiedler, J. High Energy Phys. 02 (2014) 078.
[21] G. Somogyi, J. Math. Phys. (N.Y.) **52**, 083501 (2011); V. Del Duca, G. Somogyi, and Z. Trocsanyi, J. High Energy Phys. 06 (2013) 079; G. Somogyi, J. High Energy Phys. 04 (2013) 010.
[22] Z. Bern, M. Czakon, L. J. Dixon, D. A. Kosower, and V. A. Smirnov, Phys. Rev. D **75**, 085010 (2007).
[23] Z. Bern, M. Czakon, D. A. Kosower, R. Roiban, and V. A. Smirnov, Phys. Rev. Lett. **97**, 181601 (2006).
[24] D. Bak, H. Min, and S. J. Rey, Phys. Rev. D **81**, 126004 (2010).
[25] B. Ananthanarayan, J. Bijnens, S. Ghosh, and A. Hebbar, Eur. Phys. J. A **52**, 374 (2016).
[26] G. van Oldenborgh, Comput. Phys. Commun. **66**, 1 (1991).
[27] A. van Hameren, Comput. Phys. Commun. **182**, 2427 (2011).
[28] R. K. Ellis and G. Zanderighi, J. High Energy Phys. 02 (2008) 002.
[29] A. Denner, S. Dittmaier, and L. Hofer, Comput. Phys. Commun. **212**, 220 (2017).
[30] J. Fleischer, T. Riemann, and V. Yundin, *Proc. Sci.*, LL 2012 (2012) 020 [arXiv:1210.4095].
[31] T. Binoth and G. Heinrich, Nucl. Phys. **B585**, 741 (2000).
[32] S. Borowka and G. Heinrich, *Proc. Sci.*, LL 2012 (2012) 037.
[33] S. Borowka, J. Carter, and G. Heinrich, Comput. Phys. Commun. **184**, 396 (2013).
[34] S. Borowka, G. Heinrich, S. P. Jones, M. Kerner, J. Schlenk, and T. Zirke, Phys. Chem. Comm. **196**, 470 (2015),
[35] A. V. Smirnov, Comput. Phys. Commun. **204**, 189 (2016).
[36] F. V. Tkachov and V. V. Vlasov, Report No. MCGILL-91-04; A. N. Kuznetsov and F. V. Tkachov, Report No. NIKHEF-H-90-17.
[37] A. Freitas, J. High Energy Phys. 07 (2012) 132; 09 (2012) 129(E).
[38] D. Kreimer, Mod. Phys. Lett. A **09**, 1105 (1994).
[39] L. Brucher, J. Franzkowski, and D. Kreimer, Comput. Phys. Commun. **115**, 140 (1998).
[40] J. Fleischer, V. A. Smirnov, A. Frink, J. G. Korner, D. Kreimer, K. Schilcher, and J. B. Tausk, Eur. Phys. J. C **2**, 747 (1998).
[41] A. Freitas, J. High Energy Phys. 07 (2012) 132.
[42] S. Becker, C. Reuschle, and S. Weinzierl, J. High Energy Phys. 12 (2010) 013.
[43] Z. Nagy and D. E. Soper, J. High Energy Phys. 09 (2003) 055.
[44] S. Dittmaier, Nucl. Phys. **B675**, 447 (2003).
[45] M. Assadsolimani, S. Becker, and S. Weinzierl, Phys. Rev. D **81**, 094002 (2010).
[46] A. Freitas and Y.-C. Huang, J. High Energy Phys. 04 (2010) 074.
[47] I. Dubovyk, T. Riemann, and J. Usovitsch, `MBnumerics.m` 1.0, a MATHEMATICA package for numerical evaluation of Mellin-Barnes integrals in Minkowskian regions (to be published).
[48] I. Dubovyk, A. Freitas, J. Gluza, T. Riemann, and J. Usovitsch, Phys. Lett. B **762**, 184 (2016).
[49] D. A. Kosower, Nucl. Phys. **B506**, 439 (1997).
[50] E. Witten, AMS/IP Stud. Adv. Math. **50**, 347 (2011).
[51] M. Galassi *et al.*, *GNU Scientific Library Reference Manual*, 3rd ed., `http://www.gnu.org/software/gsl/`.
[52] W. H. Press, S. A. Teukolsky, W. T. Vetterling, and B. P. Flannery, *Numerical Recipes in C*, 2nd ed. (Cambridge University Press, Cambridge, England, 1992), Sec. IV.5.